Beni-Suef University Journal of Basic and Applied Sciences

RESEARCH

Open Access

Network pharmacology, molecular docking study, and *in vivo* validation of the wound healing activity of the Red Sea soft coral *Paralemnalia thyrsoides* (Ehrenberg 1834) ethanolic extract and bioactive metabolites

Radwa Taher Mohie el-dien[1*†], Sherif A. Maher[2†], Mohamed Hisham[3], Entesar Ali Saber[4], Amgad I. M. Khedr[5], Mostafa A. Fouad[6], Mohamed Salah Kamel[6,7] and Basma Khalaf Mahmoud[6]

Abstract

Background Wounds are a major health issue on a global scale, putting a great deal of financial, commercial, and social strain on healthcare organizations, patients, and individuals. So, this study aims to investigate the *in vitro* antioxidant activity of *Paralemnalia thyrsoides* soft coral total ethanolic extract. Also, bio-guided *in vivo* wound healing validation enhanced by the evaluation of related gene expression of *Paralemnalia thyrsoides* total extract, derived fractions, and three known metabolites was done. Furthermore, utilizing network pharmacology, we identified ten hub target genes associated with wound healing, including *AKT1(RAC-alpha serine/threonine–protein kinase), IL6 (interleukin-6), MAPK3 (mitogen-activated protein kinase 3), MMP9 (matrix metalloproteinase 9), and APP (amyloid P protein precursor)*. We conducted molecular docking to assess how the three compounds interact with these hub genes and inflammatory cytokines *(IL-1β (interleukin-1 beta), TGF-β (transforming growth factor-beta), TNF-α (tumor necrosis factor-alpha),* and *NF-KB (nuclear factor-kappa B)* linked to wound healing.

Results *In vitro* antioxidant activity of the total ethanolic extract of *Paralemnalia thyrsoides* revealed potent scavenging activity against H_2O_2 with IC_{50} of 178.62 µg/mL. Additionally, the bio-guided scheme of the *in vivo* wound healing assay leads to the most active fraction, petroleum ether, with a healing percentage of 85% ± 4. Several chromatographic procedures upon petroleum ether fraction led to the isolation of three known compounds with significant *in vivo* wound healing potential which are recognized as triacontan-1-ol (1), 24-methylcholesterol (2) 6α-acetyl-7α-acetate-1(10)-α-13-nornardosine [$C_{16}H_{24}O_4$] (3). Noteworthy downregulation in *Cox-2 (Cyclooxygenase-2), Cox-1 (Cyclooxygenase-1), IL-1β, TGF-β, TNF-α, NF-KB, and INF-ϒ (interferon-ϒ)* relative genes expression and upregulation in *TGF-β, and IL-10 (interleukin-10)* relative genes expression proved that compounds (3), (2), and (1) were, respectively, significant. The *in silico* study suggests that both $C_{16}H_{24}O_4$ and 24-methyl cholesterol have potential in wound healing, possibly involving the regulation of RAC-alpha serine/threonine-protein kinase (*AKT1*).

†Radwa Taher Mohie el-dien, Sherif A. Maher have contributed equally to this work.

*Correspondence:
Radwa Taher Mohie el-dien
Radwa.Taher88@phy.nvu.edu.eg
Full list of author information is available at the end of the article

Conclusion Our study highlights the antioxidant and wound-healing potential of *Paralemnalia thyrsoides* soft coral that can be attributed to its diverse chemical metabolites. The *in vivo* and *in silico* findings highlighted that *P. thyrsoides* can be an effective remedy for wound restoration with the need for extensive future detailed clinical studies to prove these results.

Keywords *Paralemnalia thyrsoides*, Wound healing, Spectroscopic analysis, Network pharmacology, Docking study, Histopathology examination

1 Background

Wounds are a major worldwide health problem that imposes considerable profitable, and fiscal burdens on healthcare organizations, professionals, and cases [1]. When the skin is injured, the body's natural response is wound healing, which happens in four stages: inflammation, hemostasis, proliferation, and remodeling [2]. Wounds to be healed is a complicated approach with several components. Fungi and bacteria colonize wounds quickly, slowing healing [3, 4]. The outcome, experts advise using antibacterial topical formulation as it has been proven as the most effective treatment to prevent infection of deeper bodily tissues, which can lead to death of tissues [5, 6]. Nonetheless, some topical antibiotics may cause toxicity of the cells, causing wound curing to be delayed. Moreover, resistance to antibiotics may make wound cleaning and curing more difficult [7, 8]. Because of their availability, safety, diversified biology-related activities, and distinctive secondary metabolites, there has recently been a highly increasing need for the extraction of natural compounds, whether from plants or marine sources, to treat various ailments [9].

The marine environment offers a tremendous biodiversity in their constituents, Soft corals survive in competitive and severe conditions, where they create secondary metabolites for defense [10], many of them have recently undergone preliminary and clinical trials, because of their encouraging in vivo and in vitro outcomes [11, 12]. Over 40% of the soft coral species that are known to exist worldwide are found in the Red Sea, making this coastal area a hub for marine biodiversity. Secondary metabolites found in Red Sea soft corals include sesquiterpenoids, steroids, triterpenoids, diterpenoids, various fatty acid derivatives, and ceramides. Whereas the noticeable bioactivities from these newly discovered metabolites were anticancer, antibacterial, and anti-inflammatory [12, 13]. Nor-sesquiterpenoids and Sesquiterpenoids of the nardosinane [14] and neolemnane [15, 16] types have been shown to be abundant in soft corals of the genus *Paralemnalia*. *Paralemnalia thyrsoides* (family Nephtheidae, order Alcyonacea, class Anthozoa, phylum Cnidaria) have been found to be an abundant source of sesquiterpenoids and nor-sesquiterpenoids [16–19] such as paralemnolin A-W [15, 20–22], lemnalemnanes A-C [23], paralemnanone, isoparalemnanone, and paralemnanol [24], most of these metabolites exhibited crucial in vitro anti-inflammatory, neuroprotective, and cytotoxic activities [25–27]. A growing number of research are being conducted to uncover chemicals extracted from marine organisms that are beneficial in wound curing and skin cell renewal applications [28].

Although the fact that research demonstrating anti-inflammatory activity exists of *P. thyrsoides* metabolites, very little has been discovered regarding the drug's mechanism of action concerning its capacity to heal wounds. As a result, using a surgical excision wound model, we investigated the *in vivo* and *in vitro* wound-curing efficacy of *P. thyrsoides* extract and phytochemical constituents, with a focus on significant wound-curing molecular targets such as *tumor necrosis factor* (*TNF-α*), *interleukin-1β* (*IL-1β*), *interferon-*ϒ (*INF-*ϒ), *nuclear factor-kappa* B (*NF-KB*), *transforming growth factor-β* (*TGF-β*), and *interleukin-10* (*IL-10*), results are supported by histopathological examination. Furthermore, we used Cytoscape 3.10.0 software to construct protein–protein interaction (PPI) networks, identifying and extracting the top ten significant genes based on their connectivity within the network using the Cytohubba plug-in. Subsequently, we performed an in silico molecular docking investigation with all our detected compounds, screening them versus nine particular gene domains linked to the cure of wounds.

2 Materials and methods

2.1 General experimental procedure

The instruments and reagents utilized for extraction, isolation, and structure elucidation throughout this study are described in the supplementary file in detail.

2.2 Animal material

P. thyrsoides soft coral specimens were collected by scuba divers in December 2019 from the Hurgada coast of Egypt at a depth of 12 m. The freshly collected samples were kept in a −20 °C freezer until they were extracted.

2.3 Extraction and isolation

P. thyrsoides was weighed at 730.0 gm (wet weight) and 90.0 gm (dry weight). The dried pieces were sliced and

then extracted using maceration with 70% ethanol. The extract was concentrated under reduced pressure, resulting in 48.84 gm of residue without any solvent. This residue was then fractionated using different organic solvents: pet. ether, DCM, ethyl acetate, and butanol. Each solvent was evaporated separately under vacuum, yielding four fractions weighing 12.6, 9.7, 2.0, and 15.0 gm, respectively.

A 12.6 g sample of pet ether fraction was separated using silica gel column chromatography. Initially, it was eluted with petroleum ether and then the polarity was progressively raised by 10% using EtOAc. This process resulted in the formation of eight subfractions labeled as I-VIII. Subfraction II underwent chromatography on a silica gel column using gradient mixes of petroleum ether and ethyl acetate. This process led to the separation of compounds 1 (75 mg) and 2 (50 mg). The subfraction IV underwent further chromatography using a silica gel column chromatography method. It was eluted isocratically using a mixture of pet. ether and EtOAc (92:8, v/v). This process resulted in the formation of compound 3, weighing 65.4 mg.

2.4 In Vitro antioxidant activity

2.4.1 Scavenging activity for hydrogen peroxide

The antioxidant capacity was determined by reacting a certain amount of externally provided H_2O_2 (10 mmol/liter) [29]. The residual H_2O_2 was detected using the colorimetric technique. Essentially, 20 µL of the sample was mixed with 500 µL of H_2O_2 and thereafter heated to a temperature of 37 °C for 10 min. Next, the enzyme peroxidase (HRP)/3, 5-dichloro-2-hydroxyl benzene sulfonate (500 µl) was introduced and allowed to undergo incubation at a temperature of 37 °C for 10 min. Researchers were able to detect the intensity of the colored product at 505 nm using colorimetry. This measurement enabled them to determine the percent inhibition, which indicates the sample's scavenging activity compared to the blank. As a conventional benchmark, ascorbic acid was used [30, 31].

The fraction of H2O2 scavenging activity was computed using the following formula:

$$\text{Scavenging activity} = \frac{\text{A control} - \text{A sample}}{\text{A control}} \times 100$$

The IC_{50} was calculated using four separate concentrations using the GraphPad Prism 7 software.

2.4.2 Superoxide radical scavenging activity

The Sreenivasan et al. technique was used to assess the scavenging activity of the superoxide anion [32]. The generation of superoxide anion radicals was achieved by using the Tris–HCl buffer (16 mM, pH 8.0). The mixture consisted of 0.8 mL of Tris–HCl buffer, 90 µl of NBT (0.3 mM), 90 µl of NADH (0.936 mM) solution, 0.1 mL of *P. thyrsoides* complete extract at different concentrations (125, 250, 500, and 1000 mg/mL), and 90 µl of NBT (0.3 mM) (16 mM, pH 8.0). To initiate the reaction, a volume of 0.1 mL of PMS solution with a concentration of 0.12 mM was added to the mixture. The reaction was then incubated for 5 min at a temperature of 25 °C. The optical density at 560 nm was obtained by comparing it to the reference ascorbic acid. The percentage of inhibition was calculated using the following formula:

$$\text{Superoxide scavenging activity} = \frac{\text{A control} - \text{A sample}}{\text{A control}} \times 100$$

The IC_{50} value was determined using GraphPad Prism 7 software, using four distinct concentrations.

2.5 In vivo wound healing activity

2.5.1 Wound healing assay

2.5.1.1 Animal A total of eighty adult male albino rats, with an average weight of 210 ± 50 g, were individually housed in separate cages. They were provided with a normal feed and tap water in a controlled environment maintained at a temperature of 25 °C and humidity of 55%. The rats were subjected to a twelve-hour cycle of alternating darkness and light. The Ethics Committee approved this research and stipulated that animals must not experience any kind of distress during testing and must be maintained following the guidelines outlined in the Guide for the Care and Use of Laboratory Animals.

2.5.1.2 Sample preparation for wound healing activity The total extract, various organic solvent fractions (petroleum ether, ethyl acetate, dichloromethane, butanol), and isolated compounds were prepared by dissolving 2 g of the total extract and fractions in 100 ml of a 0.5% solution of carboxymethylcellulose, while 40 mg of the isolated compounds were dissolved in 20 ml of a 0.5% solution of carboxymethylcellulose [33].

2.5.1.3 Administration and wound excision model The rats were rendered unconscious by injecting ketamine (Alphasam company®, Holland, 50 mg/kg) and xylazine hydrochloride (Alphasam company®, Holland, 10 mg/kg) into their peritoneal cavity (I.P.) [34]. The Mebo ointment, manufactured by Julphar Gulf Pharmaceutical Industries® in Ras Al Khaimah, United Arab Emirates, contains 0.25% w/w beta-sitosterol. It was used topically at a dosage of 100 mg per lesion, twice daily for 14 days, resulting in significant improvement of the wounds [35]. Following the administration of anesthetic, the rats' degree of consciousness, or alertness, was assessed and their fur was removed by shaving. The place where the animal was shaved was located in

the rear, namely at the withers. The process included the use of alcohol at a concentration of 70% and povidone-iodine at a concentration of 10%, which was repeated seven times. Before creating the incision, the animals had their hair removed from the region along the spine. The wound was made by using a biopsy punch to make a circular excision with a diameter of 6 mm [36]. This method induces a wound that affects both the outermost layer of the skin (epidermis) and the layer underneath it (dermis). A total of 80 rats were split into 10 groups, with each group consisting of 8 rats. The experimental groups were administered *P. thyrsoides* entire extract and fractions topically as a lotion twice daily, with a dosage of 2 mg per lesion, for 14 days. In contrast, the control groups were treated with isolated substances at 0.2 mg per wound until the wounds were fully healed.

The 1st group served as the negative control and did not get any treatment, resulting in a bare wound.

2nd group: group treated with the ethyl acetate fraction.

3rd group: Fraction group containing dichloromethane.

4th group: a group consisting of the proportion of butanol.

5th group: total ethanolic extract-treated group.

6th group consists of Mebo® ointment, which is used for market therapy.

7th group: Petroleum ether fraction-treated group.

8th group: Triacontan-1-ol compound (comp.1).

9th group: 24-methyl cholesterol (comp.2).

10th group: $C_{16}H_{24}O_4$ compound (comp.3).

A conventional surgical dressing was applied to the injured region, and subsequent dressings were changed with new ones on days 3, 7, and 10 [37].

2.5.1.4 Wound healing evaluation To document the physical appearance and healing progress of wounds, images of the wounded areas were captured using a digital camera (DSC-W320 Sony; Sony Corp., Tokyo, Japan) on days 0, 3, 7, 10, and 14. The camera was positioned vertically about the middle of the wound, with a distance of 6 cm. The decrease in the size of the damaged region, known as wound closure, was utilized as a measure of the effectiveness of the treatment. The outline of the excisional wound's periphery was delineated by using translucent paper after the incision was created. The degree of wound contraction was measured on days 3, 7, 10, and 14 and quantified as a percentage of the total area of the healed wound. The percentage of wound contraction was determined by applying the following formula:

$$\text{Wound closure (\%)} = \text{Area of original wound at day 0} - \text{Area at } n\text{th day}/\text{Area of original wound at day 0} \times 100$$

n: days numbers, and the day of complete wound healing (epithelialization) were also noted for each wound. In addition, a wound aspect ratio was determined to elucidate the observed differences in the form and angular orientation of wound contraction among the groups. The length-to-width ratio of the wound was determined by measuring the length (from head to tail) and width using Image J.

2.6 Gene expression analysis

2.6.1 Total RNA extraction

To extract total RNA from 50 mg of dorsal skin tissue, a method involving the use of an ultrasonic homogenizer (Sonics-Vibracell, Sonics and Materials Inc., USA) was employed. The homogenization process was carried out using 0.5 mL TRIzol reagent (Invitrogen-ThermoFisher, Amresco, LLC-Solon, USA) [38]. Total RNA was obtained from skin tissues as directed by the manufacturer's guidelines. The yield and purity of the resultant RNA were subsequently evaluated [39].

2.6.2 Real-time qRT–PCR

The Revert Aid H Minus First Strand cDNA Synthesis kit (#K1632, Thermo Scientific Fermentas, St. Leon-Ro, Germany) was employed in strict accordance with the manufacturer's guidelines, to reverse transcribe using the identical quantity of total RNA in each sample. Maxima SYBER Green (Thermo Scientific Fermentas St. Leon-Ro, Germany) and StepOne Real-Time PCR Detection System (Applied Biosystems) were used for Real-time PCR. The specific primers utilized are presented in the supplementary file in Table. S1. 2 µg of RNA per reaction was included and 30 cycles of 95 °C for 10 s and 60 °C for 60 s were used for qRT-PCR [40]. Expression of target genes was calculated and normalized to glyceraldehyde-3-phosphate dehydrogenase (*GAPDH*) as an internal control gene. Using the comparative Ct method, the relative RNA abundances were evaluated. To calculate the relative expression, formula: $2^{(-\Delta\Delta Ct)}$ was employed [41].

2.7 Histopathological analysis

The rats were given anesthesia on the 7th and 14th days. A skin biopsy was collected from the injured location, including a 5 mm margin of surrounding healthy skin. The skin tissues were preserved in a solution of neutral

buffered formalin (10%) for 2–3 days. Afterward, the tissues underwent a series of procedures to prepare them for analysis and were then enclosed in paraffin. Tissue sections of a thickness of 5 µm were created using a Microtome and then stained with hematoxylin and eosin (H&E). The stained sections were examined using a light microscope equipped with a camera to observe neovascularization, epidermis, scar, and granulation tissues, and photographs were captured.

2.8 Network pharmacology-based Analysis of *P. thyrsoides* soft coral extract in wound healing

2.8.1 Screening of P. thyrsoides soft coral metabolites related targets genes

Target genes for triacontan-1-ol, 24-methyl cholesterol, and $C_{16}H_{24}O_4$ compounds were determined using chemical resemblances, pharmacophore models, and protein interactions through a search within the Traditional Chinese Medicine Systems Pharmacology Database and Analysis Platform (TCMSP) database (https://old.tcmsp-e.com/index.php) [42], BATMAN-TCM platform (http://bionet.ncpsb.org.cn/batman-tcm/) [43], Comparative Toxicogenomics Database (CTD) (http://ctdbase.org/) [44] and Swiss Target Prediction Database (http://www.swisstargetprediction.ch/). After that, these target genes are converted into their conical gene names using the UniProt database (https://www.uniprot.org/) [45].

2.8.2 Screening of wound healing process-related target genes

Genes associated with the wound healing process were collected from the GeneCards database (https://www.genecards.org/) [46] and Comparative Toxicogenomics Database CTD (https://ctdbase.org/) databases using the keywords " wound healing, surgical wound infection, and wound infection" and the species limited to "Homo sapiens". Duplicate targets were removed, and overlapping component-related and disease-related proteins were identified based on interactivenn (http://www.interactivenn.net/) [47] intersections as potential targets of these components in the wound healing process.

2.8.3 Protein–protein interaction (PPI) network construction

We created a PPI network using STRING version 12.0 (https://string-db.org/) [48] with a list of target genes and then exported it to Cytoscape software version 3.10.0 in the United States [49], Cytoscape is a free software tool for visualizing, modeling, and analyzing molecular and genetic interaction networks, and a confidence score of 0.400 was used. Subsequently, the Cytohubba plug-in was employed to identify the top 10 significant genes within the network.

2.9 Molecular docking

We retrieved crystal structures for nine potential target genes, each with its respective Protein Data Bank (PDB) ID and resolution: AKT1 (PDB ID: 4EJN, resolution: 2.19 Å), IL6 (PDB ID: 1ALU, resolution: 1.90 Å), (PDB ID: 2ZOQ, resolution: 2.39 Å), MMP9 (PDB ID: 4XCT, resolution: 1.30 Å), TNF-α (PDB ID: 2AZ5, resolution: 2.10 Å), TGF-β (PDB ID: 6B8Y, resolution: 1.65 Å), HIF-1A (PDB ID: 3KCX, resolution: 2.60 Å), IL-1β (PDB ID: 6Y8M, resolution: 1.90 Å), and NF-kb (PDB ID: 1SVC, resolution: 2.60 Å) [50]. Subsequently, we generated input files for the identified chemical compounds, protein structures, and co-crystallized ligands using AutoDockTools [51] OpenBable v2.4 was utilized to process all ligands [52]. For the molecular docking of chemical compounds to the investigated proteins, AutoDock Vina [52, 53] was employed. Preparation of ligands and proteins Protonation is achieved by using AutoDockTools (ADT), which is a graphical user interface for preparing and analyzing ligand–protein complexes for AutoDock docking simulations. Grid boxes were defined, ensuring they did not exceed a size of 27,000 $Å^3$, and the "exhaustiveness" parameter was set at 32, which is the recommended value for small boxes. Additionally, we redocked co-crystallized ligands into the crystal structures of proteins bound to ligands to validate the docking process. The interactions between the docked drugs and the key proteins were observed and analyzed using protein-plus (https://proteins.plus).

2.9.1 Statistical analysis

GraphPad Prism 9 (La Jolla, CA), version 9.5.1, was used for the statistical analysis. The data are provided as mean ± standard deviation (SD). To assess if the data had significant variations, two-way ANOVA and one-way ANOVA were used, followed by Bonferroni's multiple comparisons tests, and a P-value equal to or less than 0.05 was found to be acceptable.

3 Results

3.1 Identification of compounds

The *in vivo* wound healing study, biologically based fractionation of the total extract of *P. thyrsoides* revealed that the pet. ether fraction demonstrated the highest significant efficacy with a healing percentage of 85% ± 4, owing to the identification of the metabolites, responsible for this potential activity, A series of chromatographic separations together with spectroscopic

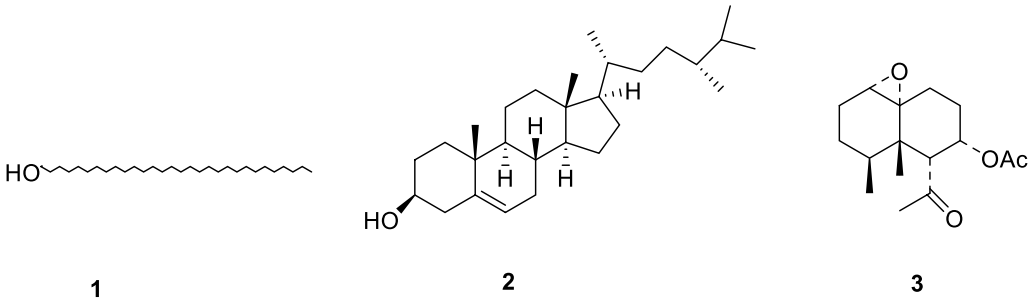

Fig. 1 Isolated compounds from the pet. ether fraction of *P. thyrsoides* soft coral

analysis yielded three known compounds, identified as triacontan-1-ol (1) [54], 24-methyl cholesterol (2) [55, 56], first reported from the genus, and 6α-acetyl-7α-acetate-1(10)-α-13-nornardosine [$C_{16}H_{24}O_4$] (3), previously isolated from the species [12, 18] shown in Fig. 1. The full ^{1}H-NMR and ^{13}C-NMR data have been compared with the previous literature (Figure S1:S8).

Compound **1:** White amorphous powder: ESI–MS: *m/z* 456 $[M+H_2O]^+$; corresponding to the molecular formula $C_{30}H_{62}O$ ^{1}H–NMR ($CDCl_3$, 400 MHz): $\delta_H = 3.64$ (2H, t, $J = 6.5$ Hz, H-1); 1.65 (2H, t, $J = 6.8$ Hz, H-2); 1.28 (m, H-3 ~ H-29); 0.88 (3H, t, $J = 6.0$ Hz, H-30); ^{13}C–NMR ($CDCl_3$, 100 MHz): $\delta_C = 65.19$ (C-1); 34.26 (C-2); 25.04 (C-3); 29.27 ~ 29.84 (C-4 ~ C-27); 32.07 (C-28); 14.26 (C-30).

Compound **2**: Colorless needles: the molecular formula was determined to be $C_{28}H_{48}O$ by El-MS spectrum (*m/z* 400.26) $[M]^+$. ^{1}H-NMR ($CDCl_3$, 400 MHz): $\delta_H = 0.79$ (3H, d, $J = 6.68$ Hz, H-26), 0.95 (3H, d, $J = 5.21$ Hz, H-21), 0.73 (3H, s, H-18), 0.85 (3H, d, $J = 6.12$ Hz, H-27), 0.79 (3H, d, $J = 6.76$ Hz, H-28), 1.03 (3H, s, H-19), 3.50 (1H, m, H-3), 5.36 (1H, d, $J = 5.12$, H-6).^{13}C–NMR ($CDCl_3$, 100 MHz) $\delta_C = 37.41$ (C-1), 31.81 (C-2), 71.96 (C-3), 42.45 (C-13, C-4), 140.89 (C-5), 121.86 (C-6), 32.06 (C-7), 34.68 (C-8), 50.29 (C-9), 36.66 (C-10), 21.22 (C-11), 39.85 (C-12), 56.96 (C-14), 24.43 (C-15), 28.04 (C-16), 56.16 (C-17), 12.00 (C-18), 19.54 (C-19), 36.33 (C-20), 19.04 (C-21), 33.87 (C-22), 30.73 (C-23), 39.22 (C-24), 30.90 (C-25), 17.74 (C-26), 20.81 (C-27), 15.59 (C-28).

Compound **3**: Oily liquid: the molecular formula was confirmed to be $C_{16}H_{24}O_4$ through ^{1}H-NMR, ^{13}C-NMR, and 2D-NMR (HSQC and HMBC). ^{1}H-NMR ($CDCl_3$, 400 MHz): $\delta_H = 2.79$ (1H, d, J = 3.68, H-1), 1.81 (2H, m, H-2), 1.19 (2H, m, H-3), 1.79 (1H, M, H-4), 3.19 (1H, d, J = 6.12, H-6), 5.31 (1H, dd, J = 10.7 &4.5, H-7), 1.16 &2.25 (2H, m, H-8), 2.21&1.18 (2H, m, H-9), 2.27 (3H, s, H-12), 0.73 (3H, d, J = 6.8, H-13), 1.05 (3H, s, H-14), 1.96 (3H, s, OAc). ^{13}C–NMR ($CDCl_3$, 100 MHz) $\delta_C = 57.17$ (C-1), 21.30 (C-2), 24.16 (C-3), 29.90 (C-4), 40.11 (C-5), 57.58 (C-6), 70.97 (C-7), 24.36 (C-8), 29.06 (C-9), 61.99 (C-10), 208.41 (C-11), 33.52 (C-12), 15.59 (C-13), 17.14 (C-14), 169.92 & 21.06 (OAc).

3.2 Antioxidant activity *in vitro*

3.2.1 Scavenging activity for hydrogen peroxide

Drugs with antioxidant effects are expected to reduce the oxidative stress of wounds and accelerate wound healing. They serve an important function in limiting the impairment of biological components caused by reactive oxygen species (ROS). *P. thyrsoides* soft coral antioxidant activity (AA) scavenging capability versus H_2O_2 was investigated in this work. The whole extract of *P. thyrsoides* prevented the production of H_2O_2 radicals in a manner that was dose-related, at 1000 µg/

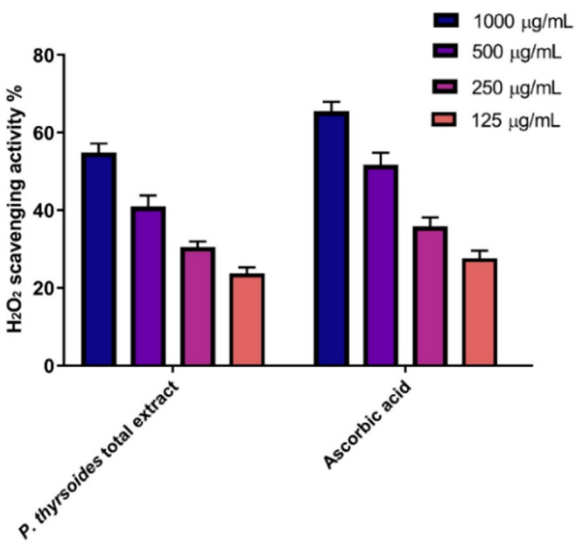

Fig. 2 Total ethanolic extract of *P. thyrsoides* soft coral, and ascorbic acid as standard reference H_2O_2 radical scavenging activity at various doses (125, 250, 500, 1000 µg/ml). The bars show the mean ± standard deviation (SD). A significant difference between groups is examined using a two-way ANOVA after variables have been normalized using the Shapiro–Wilk test

mL, the highest hydrogen peroxide radical scavenging activity was 54.86% and showed consistent AA with an IC_{50} of 178.62 µg/mL, in comparison with ascorbic acid (IC_{50} = 181.4 µg/mL) as the standard antioxidant (Fig. 2).

3.2.2 The activity of superoxide radical scavenging

Healthy wound recovery is aided by oxidation–reduction signaling and enhanced oxidative stress, both of which promote inflammation, hemostasis, granulation tissue formation, angiogenesis, extracellular matrix production, maturation, and wound closure [57]. Since soft coral *P. thyrsoides*' superoxide scavenging capability was assessed, the findings revealed that raising the concentrations enhanced the scavenging effectiveness of the ascorbic acid and extract shown in Fig. 3. *P. thyrsoides* whole extract had the highest superoxide radical scavenging activity, with 71% effectiveness at a concentration of 1000 µg/mL. The concentration of the total extract of *P. thyrsoides* required for 50% inhibition (IC_{50}) was determined to be 157.7 µg/mL in comparison with standard ascorbic acid (IC_{50} = 162.8 µg/mL).

3.3 Activity of wound healing

3.3.1 Estimation of wound closure rate

Our bio-guided study of *P. thyrsoides* soft coral total extract and different fractions revealed that wounds to be cured and closed increased in all rats in a manner that was time-related. Group 7 was the most active fraction till the end of the experiment (14th day) with a healing percentage of 85.6% ± 2.66 compared with group 6 with a healing percentage of 60.6% ± 2.66.

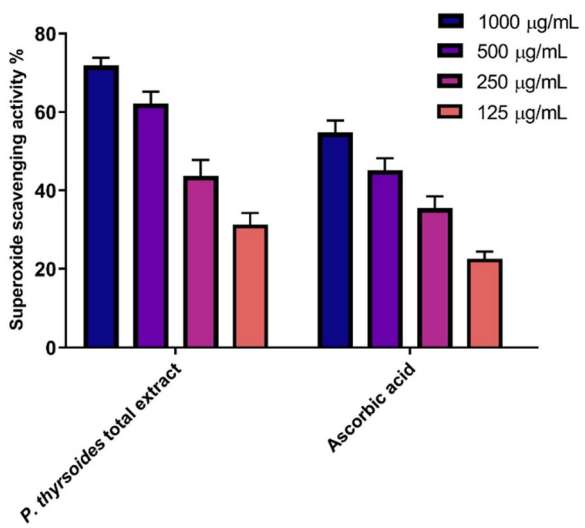

Fig. 3 Total ethanolic extract of *P. thyrsoides* soft coral superoxide radical scavenging activity at various does (125, 250, 500, and 1000 µg/mL). The bars show the mean ± standard deviation (SD). A significant difference between group is examined using a two-way ANOVA test after variables have been normalized using the Shapiro–Wilk test

Based on that, the results of the wound healing activity of the petroleum ether fraction metabolites showed that the wound closure rate on the 3rd day was around 10.5 to 45.6% in every group, with the lowest percentage in group 1 that did not receive any treatment and the highest one in the treated groups but without significance (p more than 0.05), but wounds to be cured and healed seemed to be considerably higher (p less than 0.05) in the group 10, and group 9 than in the matching untreated group. However, in the seven day after wound treatment, the wounds to be cured and healed in group 10, and group 9 seemed to be considerably greater (p less than 0.05) than the matching group that did not receive any treatment, shown in Fig. 4.

Furthermore, group 10, and group 9 had rapid wound healing rates than group 6 (p less than 0.05). The wounds to be closed and healed in group 10, group 9, and group 8 were again considerably greater (p less than 0.05) than the matching group that did not receive any treatment in the ten day after wound treatment. Finally, in the fourteen day after wound treatment, the healing percentages in group 9 and group 8 were 94.5% ± 2.45% and 90.13% ± 2.53%, respectively. The complete healing in the wounds treated with group 10 reached 97% ± 1.31%, shown in Fig. 5A. To clarify the observed differences in the shape (circular, longitudinal, or any other shapes), and direction of wound contraction between groups, we calculate the wound aspect shape ratio (length: width) in Fig. 5B.

3.3.2 Effect of P. thyrsoides soft coral on relative gene expression of IL-1β, TNF-α, Cox-1, Cox-2, NF-KB, INF-ϒ, IL-10, and TGF-β

Figure 6A depicts the mRNA expression of *Cox-1*, and *Cox-2* following excisional wound therapy with *P. thyrsoides* soft coral total extract-, derived fractions-, and compounds-treated groups along with Mebo® -treated group. *Cox-2*, and *Cox-1* relative gene expression in skin tissues was considerably reduced in wounds treated with $C_{16}H_{24}O_4$, 24-methyl cholesterol, and Triacontan-1-ol compounds for seven or fourteen days than in the group that did not receive any treatment (p less than0.05). Also, the relative expression of *Cox-2*, and *Cox-1* in wounds treated with $C_{16}H_{24}O_4$, 24-methyl cholesterol, and Triacontan-1-ol compounds, showed a greater decrease in the mRNA expression in comparison with the group treated with Mebo® (market treatment).

The mRNA expression of *TNF-α* and *IL-1β* is shown in Fig. 6B. Cytokines such as *TNF-α* and *IL-1β* inflammatory marker activity was considerably reduced in

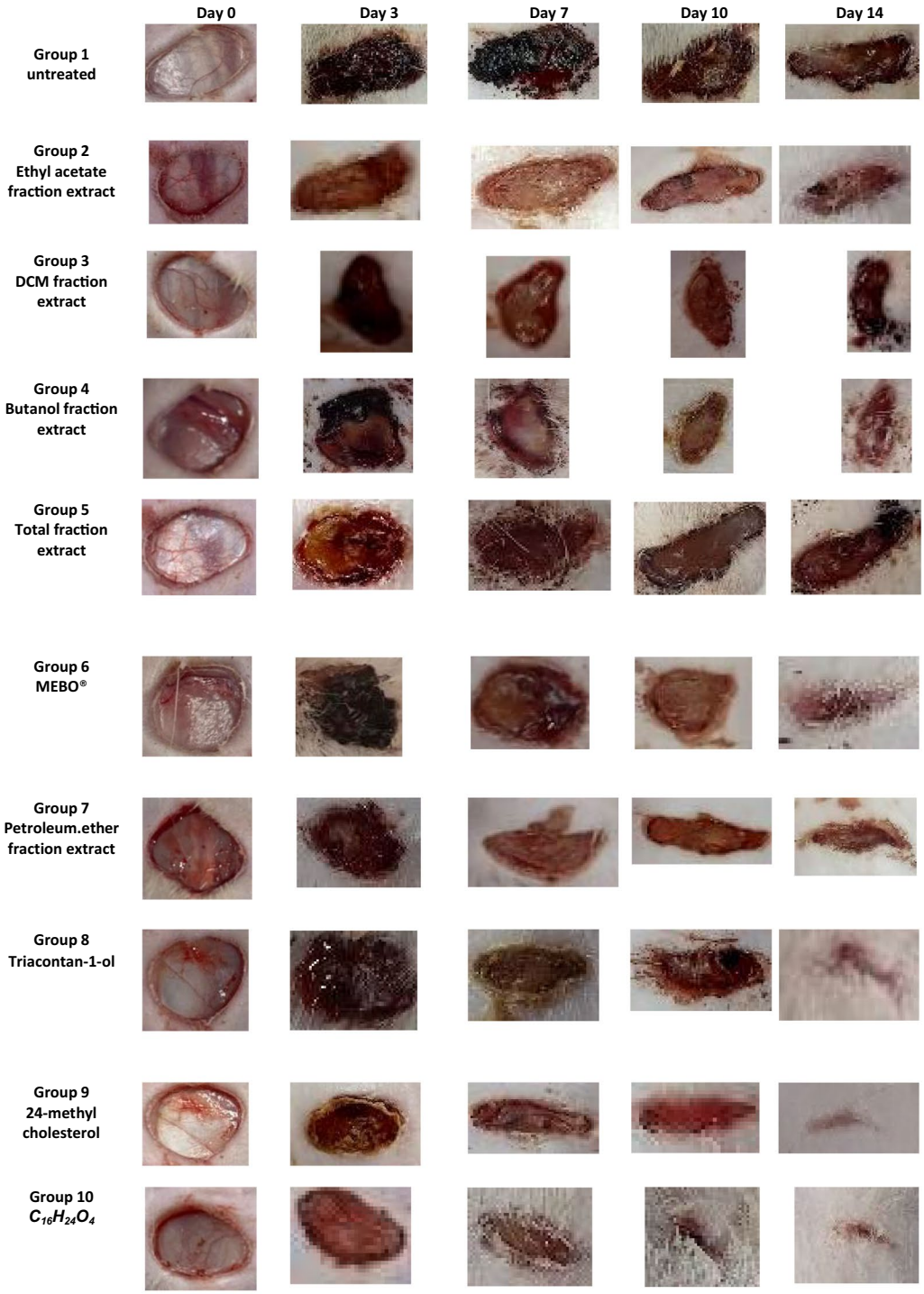

Fig. 4 Excisional wound activity for *P. thyrsoides*-treated groups and Mebo® in adult male albino rats on days zero, three, seven, ten, and fourteen post-wounding

wounds treated with $C_{16}H_{24}O_4$, 24-methyl cholesterol, Triacontan-1-ol compounds-treated wounds, petroleum ether fraction, total extract, butanol fraction, dichloromethane fraction, ethyl acetate fraction of *P. thyrsoides* soft coral, respectively, compared to untreated wounds on day 7 post-injury. In comparison with the group treated with Mebo® ointment, injured rats with $C_{16}H_{24}O_4$ compound treatment showed a

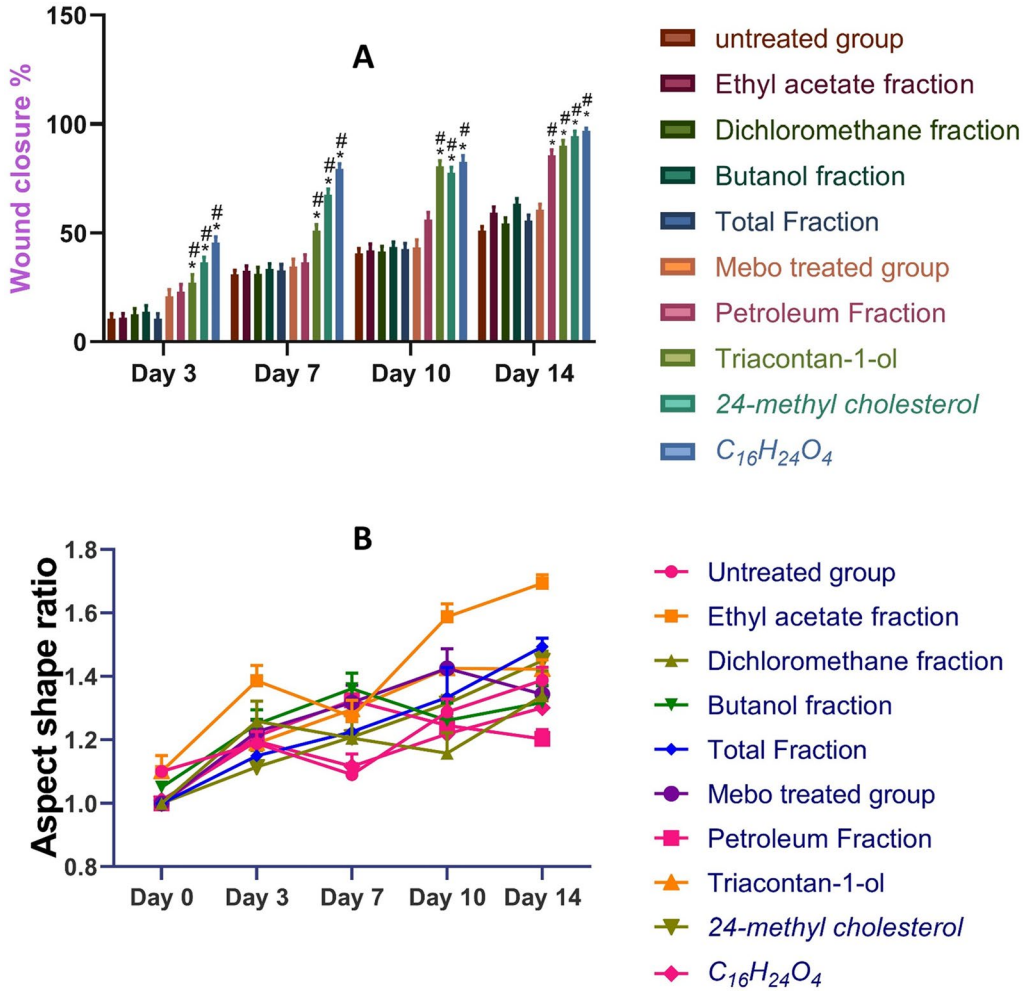

Fig. 5 **A** Wound closure rates in all studied groups after damage. Data were reported as mean ± standard deviation. *$p < 0.05$ compared to the matching group on the respective day and #$p < 0.05$ compared to the Mebo® group on the corresponding day. **B** The wound aspect ratio (Length: width) was calculated to reflect observed differences in the form and direction of wound contraction across groups

considerably greater decrease in (*IL-1β*, and *TNF-α*). Furthermore, in comparison with the group that did not receive any treatment, $C_{16}H_{24}O_4$, 24-methyl cholesterol, and Triacontan-1-ol compounds-treated wounds, respectively, for fourteen days revealed a significant reduction in *IL-1β* and *TNF-α* relative expression in comparison with the group did not receive any treatment at (p less than 0.05).

The relative gene expression of *INF-*ϒ and *NF-KB* is depicted in Fig. 6C. Analysis of the relative expression of *INF-*ϒ and *NF-KB* in full-thickness wound samples on day 7 post-injury revealed significantly lower levels in wounds treated with $C_{16}H_{24}O_4$, 24-methyl cholesterol, and Triacontan-1-ol, petroleum ether fraction, total extract, butanol fraction, dichloromethane fraction, ethyl acetate fraction of *P. thyrsoides* soft coral, respectively, in comparison with the wounds did not receive any treatment. Injured skin tissue rats treated with the $C_{16}H_{24}O_4$ compound, in comparison with rats treated with Mebo® ointment, show a substantial decrease in relative gene expression. Furthermore, $C_{16}H_{24}O_4$, 24-methyl cholesterol, and Triacontan-1-ol-treated wounds for fourteen days revealed a substantially greater decrease in relative gene expression than wounds that did not receive any treatment (p less than 0.05). Lastly, mRNA relative gene expression of *NF-KB* and *INF-*ϒ in wounds treated with $C_{16}H_{24}O_4$, 24-methyl cholesterol, and Triacontan-1-ol was substantially lower than in Mebo®-treated wounds (market therapy).

Figure 6D shows the mRNA relative gene expression of anti-inflammatory markers *transforming growth factor-beta*, and *interleukin-10* after excisional wound care with $C_{16}H_{24}O_4$, 24-methyl cholesterol, and Triacontan-1-ol-treated groups, petroleum ether fraction, total extract,

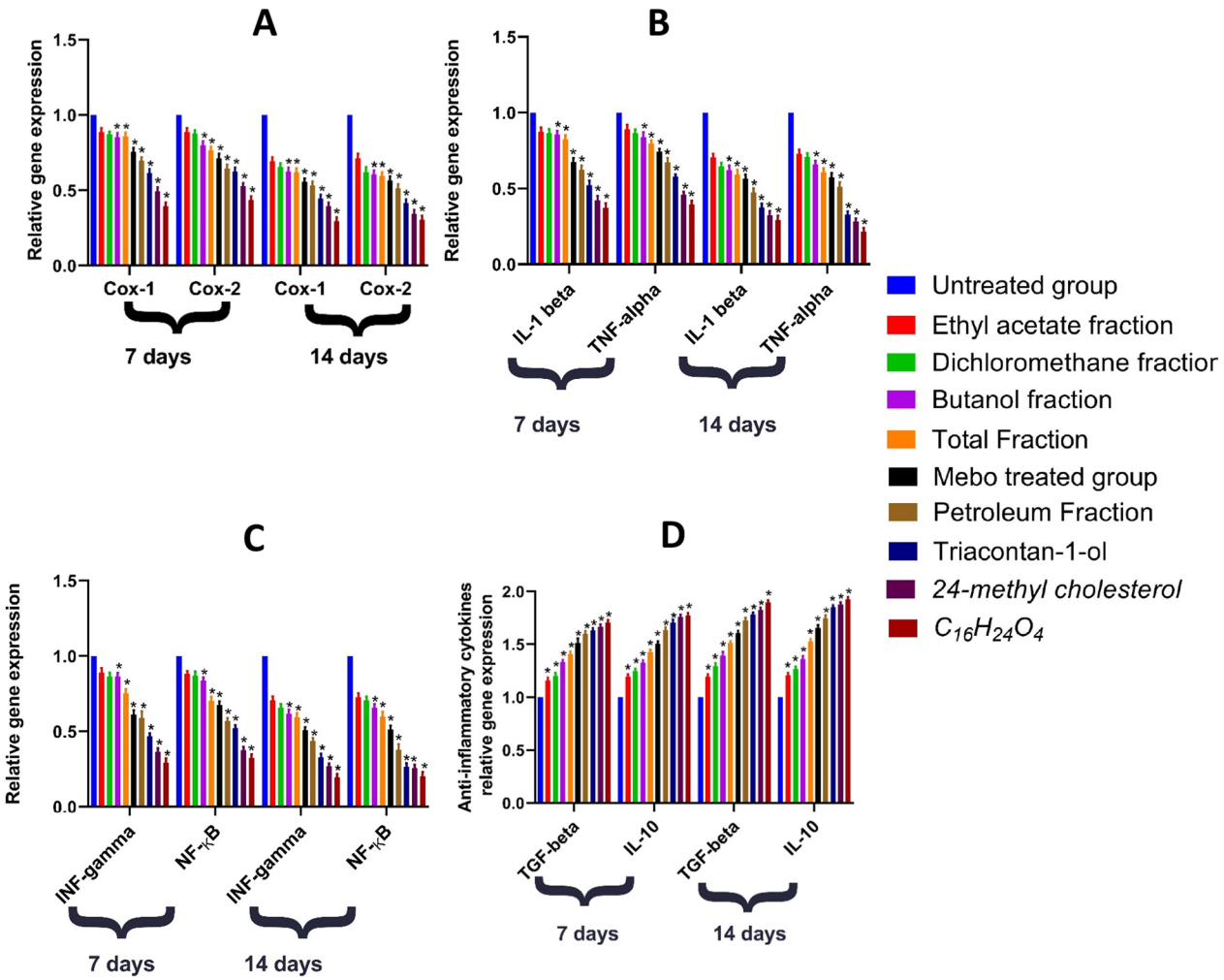

Fig. 6 The relative genes expression of *Cox-1, and Cox-2* (**A**) *TNF-α* and *IL-1β* (**B**) *INF-γ and NF-KB* (**C**) and *IL-10, TGF-β* (**D**) in different study groups. After normalization to *glyceraldehyde 3-phosphate dehydrogenase* (*GAPDH*), with *$p < 0.05$ compared to the untreated group on the relevant day

ethyl acetate fraction, dichloromethane fraction, butanol fraction of *P. thyrsoides* soft coral*, and* Mebo®-treated group. *IL-10* and *TGF-β* relative mRNA gene expression in tissues of skin was significantly greater in $C_{16}H_{24}O_4$, 24-methyl cholesterol, Triacontan-1-ol, petroleum ether fraction, and the total extract-treated groups, respectively, for the seven and/or fourteen days in comparison with the group did not receive any treatment (*p* less than 0.05).

3.4 Histopathological Study

3.4.1 7 days after treatment

In group I, the histopathological study showed that blood clot blocking the wound (blood clot), congested blood capillaries (arrows), and inflammatory cells infiltration at the wound base shown in "Fig. 7A". while in group II, the histopathological study showed that the wound bed filled with sloughed granulation tissue with edema, cellular debris, extravasated RBCs. Inflammatory cells mainly neutrophils (double arrows), and disorganized compact collagen bundles (blue arrows) are seen in "Fig. 7B". Additionally, in group III the wound edges appear closer (thick arrow) and the wound bed is crowded with inflammatory cells mainly macrophages (red arrows) shown in "Fig. 7C". However, in group IV, the wound appears with closer edges covering the defect (tailed arrows). The wound base shows congested blood vessels (BV) and filled with irregular and disorganized collagen bundles shown in "Fig. 7D". Moreover, in group V, epithelial repair is observed (thick arrow) and the underlying granulation tissue (stars) containing a higher number of macrophages (red arrows in the inset) shown in "Fig. 7E". besides, in group VI, 1–2 layers of the epidermis covered with scare tissue blocking the wound (curved arrow) and

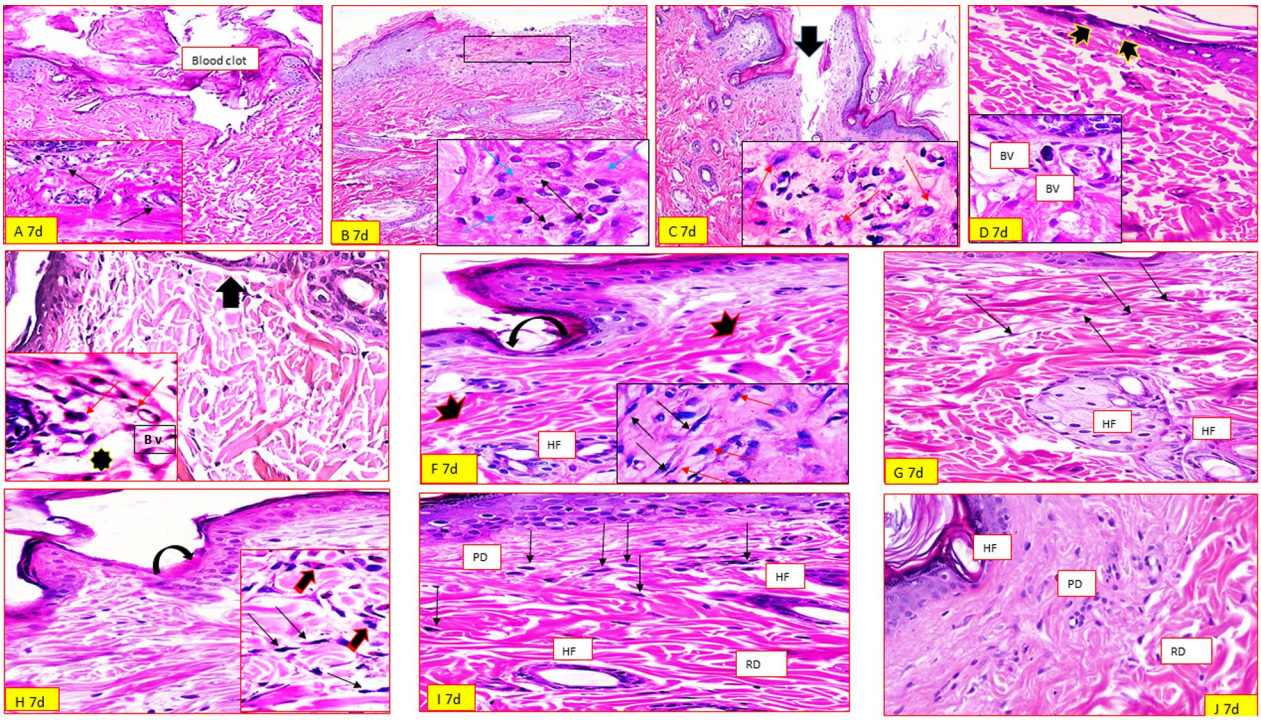

Fig. 7 **A–J** Showing wounded skin 7 days after incision (H & E stain × 200 & 400)

the dermal connective tissue has discontinuous collagen bundles (tailed arrows). Notice marked presentation of elongated, spindle-shaped fibroblasts (black arrows), myofibroblasts with acidophilic cytoplasm (red arrows) and newly formed hair follicles (HF) shown in "Fig. 7F". Furthermore, in group VII, 1–3 epithelial layers covering the wound and the underlying connective tissue containing myofibroblasts with acidophilic cytoplasm (arrows) and newly formed hair follicles (H.F) shown in "Fig. 7G". Also, group VIII showed incomplete re-epithelialization about 2–3 epithelial cell layers (curved arrow) and elongated spindle-shaped fibroblasts (black arrows) and macrophages with acidophilic cytoplasm (striped arrows) shown in "Fig. 7H". Moreover, group IX showed that more or less normal epidermis and the dermal matrix containing well-organized fibroblasts (arrows) and many hair follicles (HF) "Fig. 7I". Finally, in group X, the histopathological study showed that typical stratified squamous keratinized epithelium. Collagen bundles of the papillary dermis (PD) appeared thin irregular & disorganized and that of the reticular layer (RD) appeared as coarse wavy bundles and containing many hair follicles (HF) shown in "Fig. 7J".

3.4.2 14 Days after treatment

In the group I, the histopathological study showed that red granulation tissue fills the wound bed (stars) containing injured blood vessels with extravasated RBCs & inflammatory cells mainly eosinophils & neutrophils (red arrows) shown in "Fig. 8A", while in group II, the wound surface showed that abnormal epidermal cell growths (arrow) and the base showing granulation tissue (stars) and disorganized compact collagen bundles (tailed arrows) shown in "Fig. 8B". Additionally, in group III it showed that creeping of epidermal cells trying to cover the wound and the wound base containing granulation tissue (GT) containing numerous macrophages (red arrows) shown in "Fig. 8C". However, in group IV, epithelium repair is incomplete and covered with crust tissue (star). The dermal C.T containing frequent basophilic spindle-shaped fibroblasts (arrows) and newly formed hair follicles (HF) shown in "Fig. 8D". Moreover, in group V, inflammatory cells mainly macrophages observed, predominant fibroblasts (red arrows) and discontinuous collagen bundles filling the bottom of the wound (tailed arrows) shown in "Fig. 8E". Besides, in group VI, it showed that the epidermis formed of 1–2 cell layers, the papillary dermis containing numerous basophilic fibroblasts & macrophages with acidophilic cytoplasm (arrows) and newly formed hair follicles (HF) shown in "Fig. 8F". Furthermore, group VII showed that 1–2 epithelial layers covering the wound and the underlying connective tissue containing prominent acidophilic myofibroblasts (arrows) separated by discontinuous

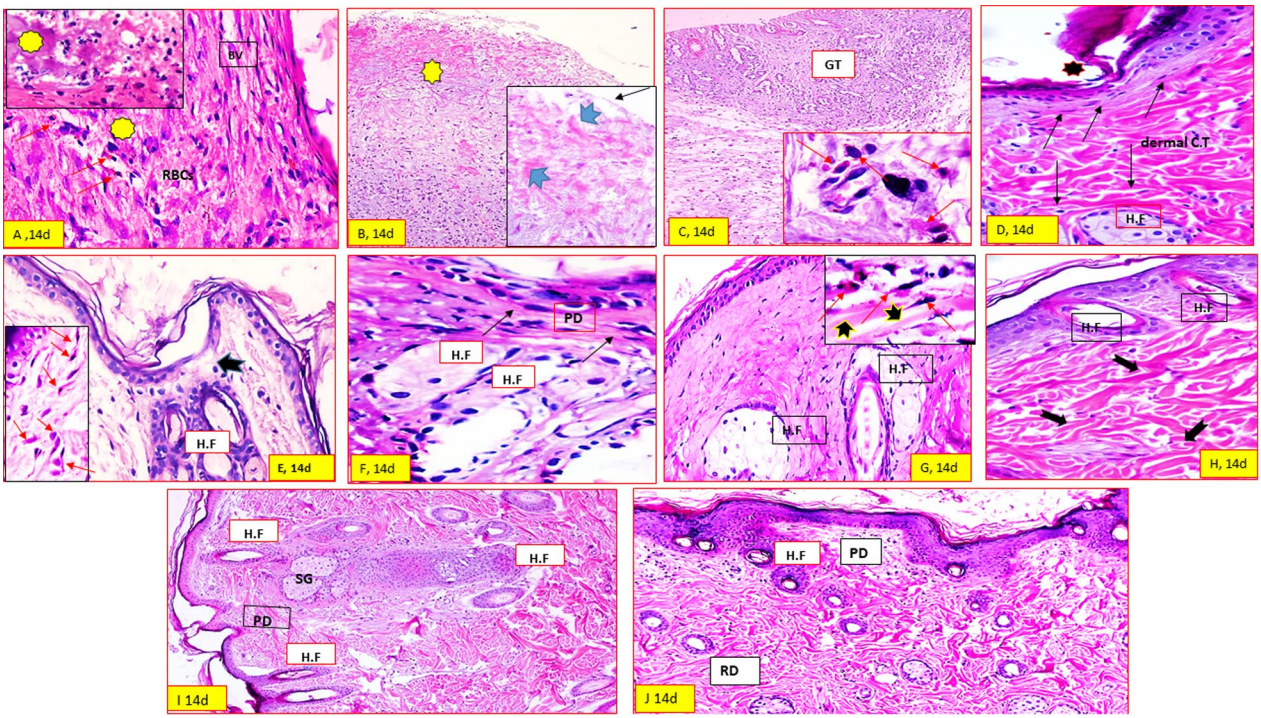

Fig. 8 **A–J** Showing wounded skin 14 days after incision (H & E stain × 200 & 400)

collagen bundles (tailed arrow) and newly formed hair follicles (H.F) shown in "Fig. 8G". Also, group VIII showed incomplete re-epithelialization (2–3 cell layers) and the papillary dermis (PD) showed newly formed hair follicles (H.F) and discontinuous collagen bundles (thick arrows) shown in "Fig. 8H". Moreover, in group IX, the wound surface showed typical stratified squamous keratinized epithelium, hair follicles, and sebaceous glands (SG). Collagen bundles of the papillary dermis (PD) appeared thin irregular & disorganized and that of the reticular layer (RD) appeared as coarse wavy bundles shown in "Fig. 8I". Finally, in group X the skin appeared more or less normal; the epidermis was formed of many cell layers, and the dermal matrix contained many hair follicles. The collagen bundles of the papillary dermis appeared thin irregular and disorganized and that of the reticular layer appeared as coarse wavy bundles shown in "Fig. 8J".

3.5 Network Pharmacology-based Analysis of *P. thyrsoides* soft coral metabolites in wound healing

3.5.1 Screening of P. thyrsoides soft coral extract-related targets genes

Predicted 453 target genes related to triacontan-1-ol, 24-methyl cholesterol, and 6α-acetyl-7α-acetate-1(10)-α-13-nornardosine [$C_{16}H_{24}O_4$] compounds were collected from TCMSP, CTD, and Swiss Target Prediction and these genes were converted into their conical gene names using the UniProt database.

3.5.2 Screening of wound healing process-related target genes

A total of 735 common target genes known to play a role in wound healing were gathered from GeneCards, CTD, and disgenet databases using the keywords "wound healing, surgical wound infection, and wound infection" and the species limited to "Homo sapiens". Duplicate targets were removed, and the Venn diagram was created to compare the targets regulated by *P. thyrsoides* extracted compounds and the potential targets for wound healing, it revealed a total of 71 common intersection targets in Fig. 9.

3.5.3 Protein–protein interaction (PPI) network construction

The 71 overlapping target genes were imported into the STRING database to perform an analysis of protein–protein interactions (PPI). The results were used to generate a PPI network diagram using the Cytoscape 3.10.0 software, resulting in 58 nodes (after excluding thirteen nodes that were not connected), 253 edges, and the average node connectivity was found to be 8.72 as depicted in Fig. 10. Afterward, the Cytohubba plug-in was employed to identify and extract the top

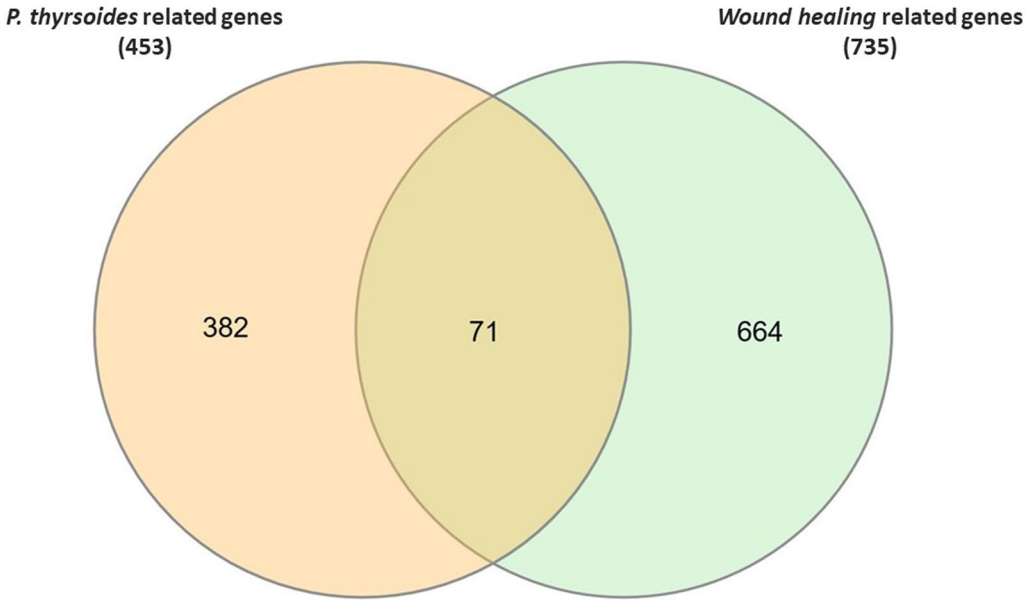

Fig. 9 Venn diagram for the integrated analysis of the related targets of *P. thyrsoides* extracted compounds and wound healing

ten significant genes based on their degree of connectivity in the network as depicted in Fig. 11, namely *AKT1, IL6, MAPK3, MMP9, HIF1A, MTOR, PPARG, ESR1, PPARA* and *APP*. We summarized the topological parameters such as node degree, betweenness, and closeness for each protein as well as skin tissue expression score in Table 1.

3.6 Molecular docking studies

Molecular docking was employed to assess the binding affinity of triacontan-1-ol, 24-methyl cholesterol, and $C_{16}H_{24}O_4$ derived from *P. thyrsoides* with the top five hub genes (*AKT-1, IL6, MAPK3, MMP9*, and *HIF1A*) as well as *IL-1β, TGF-β, TNF-α,* and *NF-KB* inflammatory cytokines. AutoDock Vina was utilized for this purpose, and the resulting binding capacity and interaction patterns were then visualized and analyzed using protein-plus (https://proteins.plus). The docking score is displayed in Table 2, where the lower the docking score (S), the stronger the binding force between the compound and the protein.

Among docked compounds, $C_{16}H_{24}O_4$ has the lowest docking energy scores ranged from −5.72 to −2.24 kcal/mol. Notably, *AKT1, HIF1A, TGF-β, MMP9* and *IL6* ranked in descending order of their docking scores, were emerged as prominent target genes demonstrating a significant binding affinity toward $C_{16}H_{24}O_4$ compound. Furthermore, 24-methyl cholesterol shows noteworthy energy score outcomes, particularly in relation to *AKT1, HIF1A, MAPK3,* and *MMP9*, with S score values of −6.27, −3.75, −3.27, and −3.05 kcal/mol, respectively. On other hand, upon docking of triacontan-1-ol shows binding affinity against *TGF-β* with docking score −2.49 kcal/mol.

In conclusion, both $C_{16}H_{24}O_4$ and 24-methyl cholesterol compounds exhibit potential in the management of wound healing by forming interactions with various target genes related to wound healing. On the other hand, RAC-alpha serine/threonine-protein kinase (*AKT1*) might have a significant role in the regulation of wound healing using these bioactive compounds. The visualizations of the lowest binding energies between *AKT1* and these bioactive compounds were created using protein-plus as illustrated in Fig. 12A-B and other docking poses of the $C_{16}H_{24}O_4$ compound with different target genes are shown in supplementary data in Figure S10.

4 Discussion

Wounds to be healed are a complicated approach that consists of the reconstruction of cells and tissue structure in the injured site as closely as possible to its natural presence [57]. According to surveys, skin wound restoration has three stages, which include an inflammatory process caused by pro-inflammatory mediators, relative expression and suppression of the immune system, a proliferative phase characterized by collagen growth, fibroblast proliferation, and formation of capillaries and vessels, and a remodeling phase characterized by cure and repair of injured dorsal skin tissue [58, 59]. As a result, drugs that may accelerate wound restoration with potential influence throughout each stage of the process,

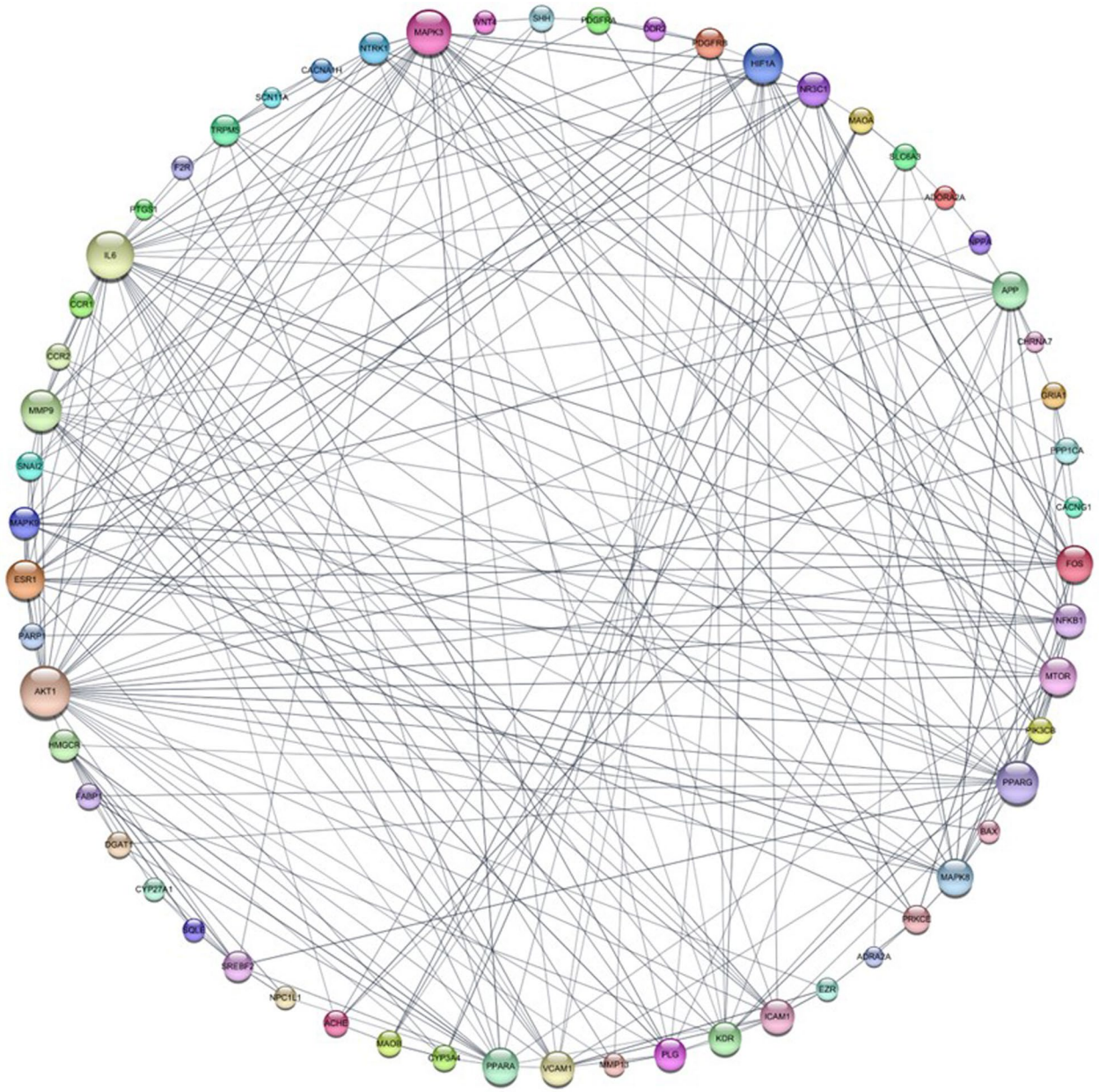

Fig. 10 Network nodes represent 58 protein targets, and the edges represent protein–protein interactions. The size of nodes signifies the connectivity of each protein, the higher the node size the higher its connectivity to other nodes

particularly those with low cost and fewer adverse effects, would be necessary for efficient therapy.

P. thyrsoides red sea soft coral is one of the terpenoid-rich soft corals with valuable biological activities, also, it is considered a member of the nardosinane-sesquiterpene producing family and possesses anti-inflammatory [60, 61], cytotoxicity [16, 62], neuroprotective [63], antifungal, and antibacterial activities [12, 64]. So in the current study, we examined the antioxidant and wound healing effect of *P. thyrsoides* total extract, fractions, and metabolites in vivo, in vitro supported by histopathological and pharmacology network studies.

Antioxidants are thought to accelerate wound healing by mitigating oxidative stress. The presence of ROS can cause significant damage to biological elements such as DNA, proteins, and lipids, but antioxidants have been shown to reduce such damage. Elevated levels of ROS, including H_2O_2 and superoxide anion, at the wound site can trigger collagen breakdown and subsequently lead to the degradation of the ECM. This, in turn, inhibits

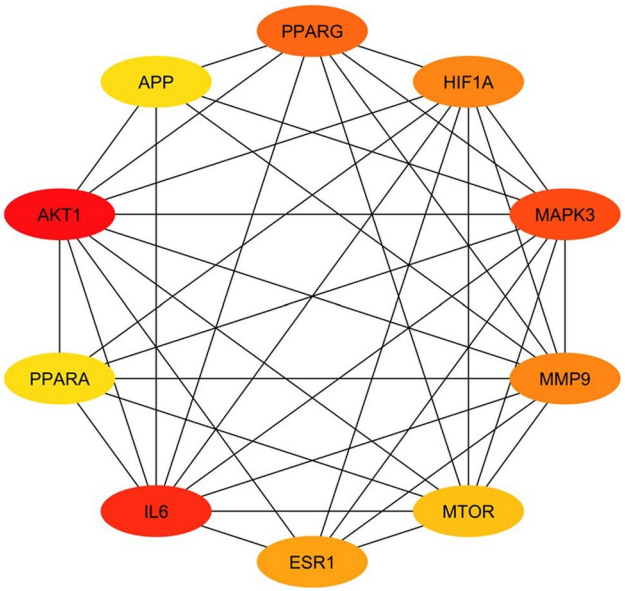

Fig. 11 Network nodes represent the top 10 hub genes: the darker the color, the higher the score and the stronger the connection

angiogenesis and re-epithelization, two critical processes necessary for wound healing [65]. Furthermore, increased ROS can lead to inflammation, which in turn raises pro-inflammatory cytokines and extends the inflammatory response [66].

P. thyrsoides soft coral's antioxidant activity of the total ethanolic extract can be explained by its superoxide dismutase (SOD) activity and scavenging activity of H_2O_2 which can eliminate ROS and improve its wound-curing activity may be ascribed to its diverse secondary metabolites with the major content of different classes of terpenoids and sesquiterpenoids that exert antioxidant activity through multiple mechanisms [61, 67]. Thus, high amounts of ROS in the injured skin tissue increase collagen degradation and extracellular matrix (ECM) deterioration. Whenever the extracellular matrix deteriorates, Re-epithelization and angiogenesis are critical procedures for wounds to be healed and cured and are inhibited [68, 69]. Furthermore, increased ROS may provoke inflammation [70].

Table 1 Topological parameters of top 10 hub genes with skin tissue expression score

No	Name	Target	Degree	Betweenness	Closeness	Tissue/Skin
1	RAC-alpha serine/threonine-protein kinase	AKT1	31	0.22133	0.67059	4.479
2	Interleukin-6	IL6	29	0.18377	0.64045	3.501864
3	Mitogen-activated protein kinase 3	MAPK3	24	0.08524	0.60638	3.576941
4	Matrix metalloproteinase-9	MMP9	21	0.08094	0.58763	3.128017
5	Hypoxia-inducible factor 1-alpha	HIF1A	19	0.02174	0.54808	4.126538
6	Serine/threonine-protein kinase mTOR	MTOR	18	0.01655	0.54808	4.000566
7	Peroxisome proliferator-activated receptor gamma	PPARG	17	0.03969	0.52778	3.232146
8	Estrogen receptor alpha	ESR1	16	0.02049	0.52778	2.810398
9	Peroxisome proliferator-activated receptor alpha	PPARA	15	0.01745	0.53271	3.01666
10	Amyloid-beta A4 protein	APP	15	0.04000	0.54286	3.999192

Table 2 Molecular docking scores of *P. thyrsoides* metabolites and selected nine potential target genes related to wound healing

Compound	Binding Energy score (S) (kcal/mol)								
	AKT1	IL6	MAPK3	MMP9	HIF1A	IL-1β	TGF-β	TNF-α	NF-KB
Triacontan-1-ol	ND	ND	ND	ND	ND	ND	−2.49	ND	0.70
24-Methyl Cholesterol	−6.27	−2.51	−3.27	−3.05	−3.75	−2.17	ND	ND	−2.71
$C_{16}H_{24}O_4$	−5.72	−3.46	−3.50	−4.19	−4.97	−3.11	−4.62	−2.24	−3.38
Co-crystallized ligand	−12.06 RMSD = 1.034 A°	−5.14 RMSD = 1.46 A°	−7.65 RMSD = 0.37 A°	−6.39 RMSD = 1.42 A°	−5.11 RMSD = 0.58 A°	−5.62 RMSD = 0.193 A°	−11.69 RMSD = 0.193 A°	−5.17 RMSD = 1.40 A°	–

ND Not detected

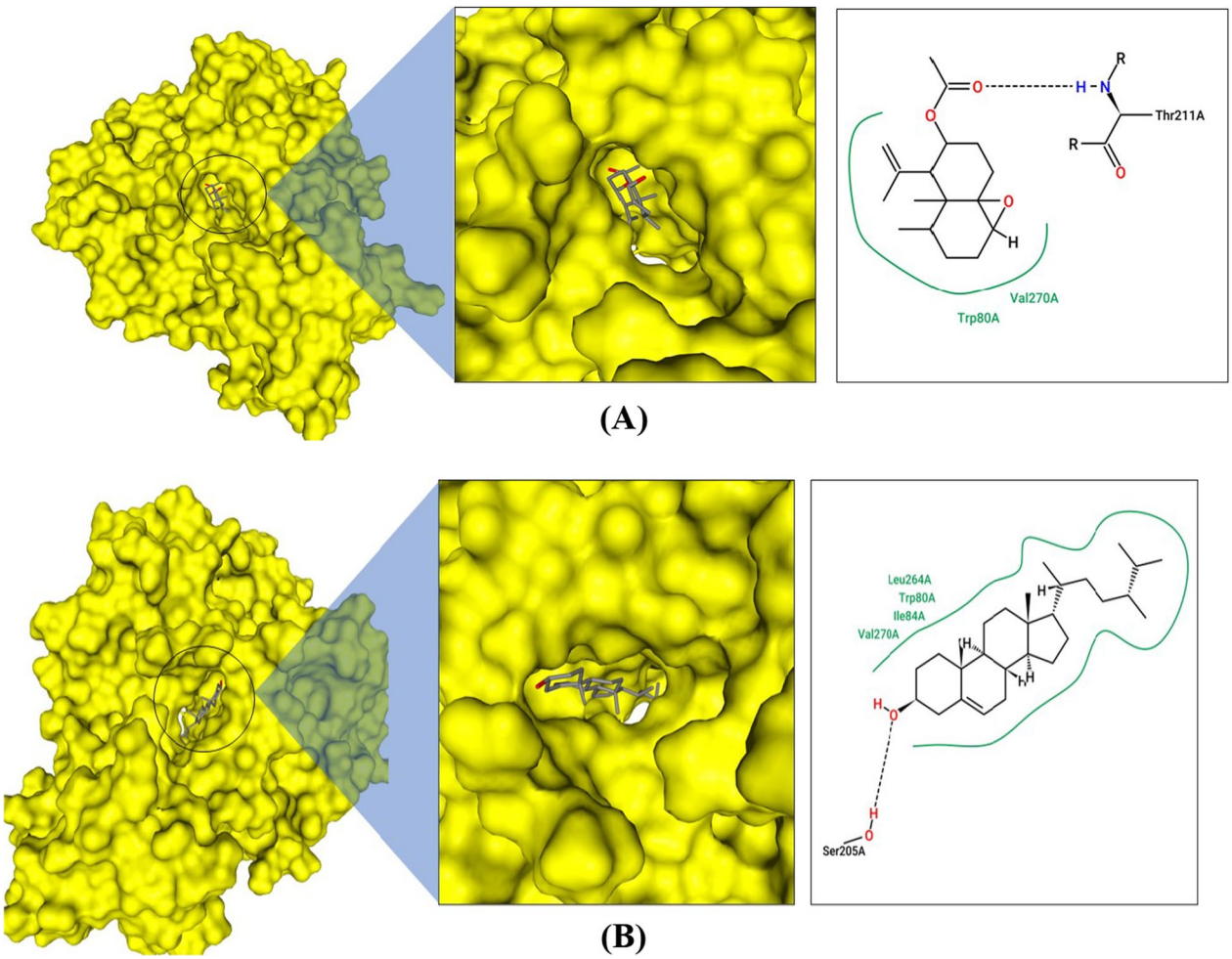

Fig. 12 Molecular docking of the key targets. The highest obtained binding poses of AKT1 with **A** $C_{16}H_{24}O_4$ and **B** 24-methyl cholesterol

The biological guided fractionation of the *P. thyrsoides* leads us to the most active petroleum ether fraction with the highest healing percentage (85.6% ± 2.66) among other treated groups even the market treated Mebo®-treated groups. In an attempt to explore the pet. ether fraction metabolites, phytochemical investigation was applied and three known metabolites were isolated and identified as triacontan-1-ol [54], 24-methylcholesterol [55, 56], and 6α-acetyl-7α-acetate-1(10)-α-13-nornardosine [$C_{16}H_{24}O_4$]. The three metabolites were tested for the *in vivo* and *in vitro* wound healing restoration ability, wound closure indicates re-epithelialization, granulation, angiogenesis, fibroblast proliferation, keratinocyte differentiation, and proliferation [71]. The marked decrease in wound area observed following $C_{16}H_{24}O_4$, 24-methyl cholesterol, and Triacontan-1-ol compounds of *P. thyrsoides* soft coral-treated groups, respectively, was confirmed through histological analysis, which demonstrated increased fibroblast proliferation, angiogenesis, and granulation tissue deposition, indicating significant re-epithelialization and collagenation in the wound bed. Besides, $C_{16}H_{24}O_4$ and 24-methyl cholesterol compounds groups had higher wound healing rates than groups treated with Mebo® ointment and untreated animals (p less than 0.05). The centripetal movement of the outermost regions of a full-thickness hole to aid in healing and tissue healing is known as wound closure [71–73].

In general, substances used to treat wounds are either able to promote the growth of fibroblasts, induce the differentiation or growth of keratinocyte cells, promote the production of collagen, or have antioxidant, and anti-inflammatory properties. When an agent possesses two or more of these biological characteristics, it may be a viable candidate for use as a wound-healing agent [66].

Additionally, wound closure is associated with *COX-1*, and *COX-2* activation in fibroblasts, cells of the mucosa, in addition to an increase in *Interlukin-1β* relative gene

expression. The results demonstrated that $C_{16}H_{24}O_4$, 24-methyl cholesterol, and Triacontan-1-ol compounds derived from pet. ether fraction-treated groups, respectively, significantly reduced the increased *COX-1*, and *COX-2* relative gene expression, confirming its protective impact in wound healing. So, the release of pro-inflammatory cytokines, such as *IL-1B* and *TNF-α*, is compulsory to boost neutrophils and exclude bacteria and other contaminants from the injured site. They are also known to be dynamic inducers of Metalloproteinase synthesis in fibroblast and inflammatory cells. Metalloproteinase degrades and removes damaged Extracellular Matrixes (ECM) during wound curing to aid in repairing the wound [74]. Also, the curing and healing processes are hampered by an inflammatory phase, *IL-1β*, and *TNF-α* and metalloproteinase harm the skin tissue, leading to the conversion of wounds from acute to chronic. *Tumor necrosis factor-α* is a growth factor released by macrophages that combines with *IL-1β* to enhance and decrease respective proliferation of fibroblasts and production of collagen [75]. *Tumor necrosis factor–alpha* promotes *NF-KB*, and *INF-*ϒ, This, in turn, enhances relative mRNA expression of a slew of *TNF-α* itself and metalloproteinase, to liberate soluble *Tumor necrosis factor–alpha* and intensify its activity [76].

On the other hand, wound-healing processes need intricate cell–cell interactions as well as multiple growth factors, especially the relative genes expression of *TGF-β* and *IL-10* are play the most important roles across every step of wound curing. *IL-10 and TGF-β* recruit and activate macrophages and neutrophils, during phases of wound healing (hemostasis and inflammation phases), whereas it promotes a variety of cellular reactions during the proliferative stage, including re-epithelialization, angiogenesis, granulation tissue formation, and extracellular matrix accumulation [77]. Also, it promotes proliferation of fibroblasts as well as transformation to myofibroblasts, which aid in wound closure during the phase of remodeling [78–80]. In the non-healing wounds due to the conversion of these wounds from acute to chronic this frequently resulted in a failure of *TGF-β* and *IL-10* relative mRNA gene expression, as Feinberg and colleagues have said that *TGF-β* and *IL-10* have an inhibitory impact on the development of collagenases, which weaken collagen and extracellular matrix [81]. These findings are consistent with the findings that $C_{16}H_{24}O_4$, 24-methyl cholesterol, and Triacontan-1-ol compounds, petroleum ether fraction, and total extract of *Paralemnalia thyrsoides* soft coral-treated groups, respectively, increased *TGF-β,* and *IL-10* relative genes expression and thus recovered wound healing. The mRNA relative gene expression of *IL-10*, and *TGF-β* increased significantly after excisional wound care with $C_{16}H_{24}O_4$, 24-methyl cholesterol, and Triacontan-1-ol compounds; additionally, these compounds showed a significant increase in the *IL-10* and *TGF-β* 's relative genes expression in comparison with the group treated with Mebo® ointment (market treatment).

Pharmacological network analysis was employed to explore the potential interactions between the wound healing-related genes and *P. thyrsoides extract-related* genes. The analysis identified the top 10 hub genes—AKT1, IL6, MAPK3, MMP9, HIF1A, MTOR, PPARG, ESR1, PPARA, and APP—based on their connectivity degree. On the other hand, additionally, molecular docking was conducted to explore molecular targets contributing to wound healing potential. The top five hub genes (*AKT-1, IL6, MAPK3, MMP9*, and *HIF1A*) as well as four examined targets (IL-1β, TGF-β, TNF-α, and NF-KB) that play a vital role in the wound healing process was employed to assess the binding affinity of triacontan-1-ol, 24-methyl cholesterol, and $C_{16}H_{24}O_4$ derived from *P. thyrsoides*. We found that $C_{16}H_{24}O_4$ had a significant binding affinity with genes like AKT1, HIF1A, TGF-β, MMP9, and IL6, crucial for wound healing. Additionally, 24-methyl cholesterol showed notable energy scores, particularly linked to genes AKT1, HIF1A, MAPK3, and MMP9. The RAC-alpha serine/threonine-protein kinase (AKT1) emerged as potentially pivotal in regulating wound healing when influenced by these bioactive compounds. These findings shed light on the complex interplay between genes and compounds, offering promising insights into enhancing wound healing mechanisms.

5 Conclusion

Marine soft corals are thought to provide a tremendous number of significant anti-inflammatory drugs. The biological investigation of the total ethanolic extract of *P. thyrsoides* revealed promising antioxidant as well as wound restoration potentials, evoking further evaluation of the different fractions (pet. ether, DCM, EtOAc, and butanol) of *P. thyrsoides*, whereas the pet. ether fraction was the most active one on wound healing activity via accelerated wound closure rate, enhancing *TGF-β* and *IL-10* and suppressing inflammatory markers (*Cox-1, Cox-2, IL-1β, TNF-α, INF-*ϒ*, and NF-KB*). Additionally, the bio-guided isolation of the pet. ether fraction metabolites resulted in the identification of three metabolites with significant wound healing potency. The aforementioned results were supported by the histopathological examination of skin tissue through more or less normal skin appearance of the pet. ether fraction and the isolated diterpene compound 6α-acetyl-7α-acetate-1(10)-α-13-nornardosine [$C_{16}H_{24}O_4$]. A network of 71 genes

associated with wound healing was established through protein–protein interactions (PPI). Among these genes, *AKT1, IL6, MAPK3, MMP9, HIF1A, MTOR, PPARG, ESR1, PPARA, and APP* demonstrated significance in terms of their connectivity within the network. Additionally, *the* in silico molecular docking studies indicate that both $C_{16}H_{24}O_4$ and 24-methyl cholesterol exhibit binding affinities toward several target genes associated with wound healing, particularly in their potential regulation of RAC-alpha serine/threonine-protein kinase (*AKT1*). Nevertheless, further investigation will be carried out to fully comprehend the mechanism of these metabolites in wound healing, in an attempt to discover new pharmaceutical drugs with lesser side effects.

Abbreviations

P. thyrsoides	*Paralemnalia thyrsoides*
Pet. ether	Petroleum ether
EtOAc	Ethyl acetate
DCM	Di chloromethane
^{1}H-NMR	Proton nuclear magnetic resonance
^{13}C-NMR	Carbon nuclear magnetic resonance
H2O2	Hydrogen peroxide
IC_{50}	Half maximal inhibitory concentration
COX-1	Cyclooxygenase-1
COX-2	Cyclooxygenase-2
IL-1β	Interleukin-1 beta
TGF-β	Transforming growth factor-beta
TNF-α	Tumor necrosis factor-alpha
NF-KB	Nuclear factor-kappa B
INF-ϒ	Interferon-gamma
IL-10	Interleukin-10
IL6	Interleukin-6
MAPK3	Mitogen-activated protein kinase 3
MMP9	Matrix metalloproteinase 9
APP	Amyloid P protein precursor
HIF-1A	Hypoxia-inducible factor 1–alpha
SOD	Superoxide dismutase
ROS	Reactive oxygen species
MTOR	Mammalian target of rapamycin
PPARG	Peroxisome proliferator-activated receptor gamma
PPARA	Peroxisome proliferator-activated receptor alpha
AKT1	RAC-alpha serine/threonine–protein kinase
ESR1	Estrogen receptor 1

Supplementary Information

The online version contains supplementary material available at https://doi.org/10.1186/s43088-024-00512-x.

Additional file 1.

Acknowledgements
The authors would like to thank Deraya university for their laboratory help.

Author contributions
M.A.F, B.K.M, S.A.M and R.T.M were involved in the conceptualization; M.A.F, B.K.M, S.A.M, and R.T.M contributed to the methodology; S.A.M, M.H, and E.A.S contributed to the software; M.A.F and B.K.M assisted in supervision; M.H, S.A.M, R.T.M and M.A.F curated the data; all authors contributed to composing and first drafting preparation; all authors write, review, and edit. The released version of the manuscript has been read and approved by all authors.

Funding
No funding.

Availability of data and materials
The data supporting the findings of this study are available upon reasonable request from the corresponding author.

Declarations

Ethics approval and consent to participate
The study complied with the Helsinki Declaration standards and was approved by the ethical review board of Deraya University's College of Pharmacy in Minia, Egypt, with approval code 13/2023. The soft coral sample was identified by Prof. Mohamed A. Abu El-Regal, Professor of Biological Oceanography, Marine Biology Department, Faculty of Marine Science, King Abdulaziz University, Jeddah, Saudi Arabia. The freshly collected samples were kept in a -20 °C freezer until they were extracted. Under the registration number Mn-Ph-Cog-065, a voucher specimen was stored in the herbarium of the Pharmacognosy Department, Faculty of Pharmacy, Minia University, Minia, Egypt.

Informed consent
Not applicable.

Competing interests
The authors state that they do not have any conflicts of interest.

Consent for publication
Not applicable.

Author details
[1]Department of Pharmacognosy, Faculty of Pharmacy, New Valley University, New Valley 72511, Egypt. [2]Department of Biochemistry, Faculty of Pharmacy, New Valley University, New Valley 72511, Egypt. [3]Department of Pharmaceutical Chemistry, Faculty of Pharmacy, Deraya University, New Minia 61111, Egypt. [4]Department of Medical Science, Histology and Cell Biology, Faculty of Pharmacy, Deraya University, New Minia 61111, Egypt. [5]Department of Pharmacognosy, Faculty of Pharmacy, Port Said University, Port Said 42526, Egypt. [6]Department of Pharmacognosy, Faculty of Pharmacy, Minia University, Minia 61519, Egypt. [7]Department of Pharmacognosy, Faculty of Pharmacy, Deraya University, New Minia 61111, Egypt.

Received: 27 December 2023 Accepted: 29 May 2024
Published online: 08 June 2024

References

1. Benbow M (2011) Wound care: ensuring a holistic and collaborative assessment. Br J Community Nurs 16(Sup9):S6–S16
2. Tanrıverdi ST, Suat B, Azizoğlu E, Köse FA (2018) In-vitro evaluation of dexpanthenol-loaded nanofiber mats for wound healing. Trop J Pharm Res 17(3):387–394
3. Xu Z, Dong M, Yin S, Dong J, Zhang M, Tian R et al (2023) Why traditional herbal medicine promotes wound healing: research from immune response, wound microbiome to controlled delivery. Adv Drug Deliv Rev 195:114764
4. Romo-Rico J, Krishna SM, Bazaka K, Golledge J, Jacob MV (2022) Potential of plant secondary metabolite-based polymers to enhance wound healing. Acta Biomater 147:34–49
5. Boateng JS, Matthews KH, Stevens HN, Eccleston GM (2008) Wound healing dressings and drug delivery systems: a review. J Pharm Sci 97(8):2892–2923
6. Hussain Z, Thu HE, Rawas-Qalaji M, Naseem M, Khan S, Sohail M (2022) Recent developments and advanced strategies for promoting burn wound healing. J Drug Deliv Sci Technol 68:103092
7. Siafaka PI, Zisi AP, Exindari MK, Karantas ID, Bikiaris DN (2016) Porous dressings of modified chitosan with poly (2-hydroxyethyl acrylate) for topical wound delivery of levofloxacin. Carbohyd Polym 143:90–99
8. Smith R, Russo J, Fiegel J, Brogden N (2020) Antibiotic delivery strategies to treat skin infections when innate antimicrobial defense fails. Antibiotics 9(2):56

9. Aly SH, El-Hassab MA, Elhady SS, Gad HA (2022) Comparative metabolic study of tamarindus indica l's various organs based on GC/MS analysis. In Silico and in vitro anti-inflammatory and wound healing activities. Plants 12(1):87
10. Kelutur F, Saptarini N, Mustarichie R, Kurnia D (2021) Bioactive compounds profile of gorgonian corals and their pharmacological activities: a review. Rasayan J Chem 14(3):1773–1789
11. Santacruz L, Hurtado DX, Doohan R, Thomas OP, Puyana M, Tello E (2020) Metabolomic study of soft corals from the Colombian Caribbean: PSYCHE and 1H-NMR comparative analysis. Sci Rep 10(1):5417
12. Elshamy AI, Mohamed TA, Elkady EM, Saleh IA, El-Beih AA, Alhammady MA et al (2021) Paralemnolins X and Y, new antimicrobial sesquiterpenoids from the soft coral paralemnalia thyrsoide. Antibiotics 10(10):1158
13. Hsu W-L, Chiu S-J, Tsai Y-T, Chang C-M, Wang J-Y, Wang ET et al (2013) A soft coral natural product, 11-episinulariolide acetate, inhibits gene expression of cyclooxygenase-2 and interleukin-8 through attenuation of calcium signaling. Molecules 18(6):7023–7034
14. Bishara A, Yeffet D, Sisso M, Shmul G, Schleyer M, Benayahu Y et al (2008) Nardosinanols A– I and Lemnafricanol, Sesquiterpenes from Several Soft Corals, Lemnalia sp., Paralemnalia clavata, Lemnalia africana, and Rhytisma fulvum fulvum. J Nat Prod 71(3):375–380
15. Huang H-C, Chao C-H, Su J-H, Hsu C-H, Chen S-P, Kuo Y-H et al (2007) Neolemnane-type sesquiterpenoids from a Formosan soft coral Paralemnalia thyrsoides. Chem Pharm Bull 55(6):876–880
16. Tseng Y-J, Lee Y-S, Wang S-K, Sheu J-H, Duh C-Y (2013) Parathyrsoidins A-D, four new sesquiterpenoids from the soft coral Paralemnalia thyrsoides. Mar Drugs 11(7):2501–2509
17. Su J-Y, Zhong Y-L, Zeng L-M (1993) Two new sesquiterpenoids from the soft coral Paralemnalia thyrsoides. J Nat Prod 56(2):288–291
18. Izac RR, Schneider P, Swain M, Fenical W (1982) New nor-sesquiterpenoids of apparent nardosinane origin from the pacific soft-coral Paralemnalia thyrsoides. Tetrahedron Lett 23(8):817–820
19. Bowden BF, Coll J, Mitchell S (1980) Studies of Australian soft corals. XIX. Two new sesquiterpenes with the nardosinane skeleton from a Paralemnalia species. Aust J Chem 33(4):885–890
20. Huang H-C, Chao C-H, Liao J-H, Chiang MY, Dai C-F, Wu Y-C et al (2005) A novel chlorinated norsesquiterpenoid and two related new metabolites from the soft coral Paralemnalia thyrsoides. Tetrahedron Lett 46(45):7711–7714
21. Wang G-H, Huang H-C, Su J-H, Wu Y-C, Sheu J-H (2010) Paralemnolins J—P, New Sesquiterpenoids from the Soft Coral Paralemnalia thyrsoide. Chem Pharm Bull 58(1):30–33
22. Phan C-S, Kamada T, Hatai K, Vairappan CS (2018) Paralemnolins V and W, new nardosinane-type sesquiterpenoids from a bornean soft coral, lemnalia sp. Chem Nat Compd 54:903–906
23. Han X, Wang Q, Luo X, Tang X, Wang Z, Zhang D et al (2021) Lemnalemnanes A-C, three rare rearranged sesquiterpenoids from the soft corals paralemnalia thyrsoides and lemnalia sp. Org Lett 24(1):11–15
24. Huang H-C, Wen Z-H, Chao C-H, Ahmed AF, Chiang MY, Kuo Y-H et al (2006) Novel sesquiterpenoids from the Formosan soft coral Paralemnalia thyrsoides. Tetrahedron Lett 47(49):8751–8755
25. Wang S-K, Lee Y-S, Duh C-Y (2012) Paralemnolide A, an unprecedented bisnorsesquiterpene from the Taiwanese soft coral Paralemnalia thyrsoides. Mar Drugs 10(7):1528–1535
26. Abdelhafez OH, Fahim JR, Desoukey SY, Kamel MS, Abdelmohsen UR (2019) Recent updates on corals from Nephtheidae. Chem Biodivers 16(6):e1800692
27. Wei W-C, Sung P-J, Duh C-Y, Chen B-W, Sheu J-H, Yang N-S (2013) Anti-inflammatory activities of natural products isolated from soft corals of Taiwan between 2008 and 2012. Mar Drugs 11(10):4083–4126
28. Sofrona E, Tziveleka L-A, Harizani M, Koroli P, Sfiniadakis I, Roussis V et al (2020) In vivo evaluation of the wound healing activity of extracts and bioactive constituents of the marine isopod Ceratothoa oestroides. Mar Drugs 18(4):219
29. Hassan H, Abdel-Aziz A (2010) Evaluation of free radical-scavenging and anti-oxidant properties of black berry against fluoride toxicity in rats. Food Chem Toxicol 48(8–9):1999–2004
30. Musa A, Shady NH, Ahmed SR, Alnusaire TS, Sayed AM, Alowaiesh BF et al (2021) Antiulcer potential of olea europea L. cv. Arbequina leaf extract supported by metabolic profiling and molecular docking. Antioxidants 10(5):644
31. Yassien EE, Hamed MM, Abdelmohsen UR, Hassan HM, Gazwi HS (2021) In vitro antioxidant, antibacterial, and antihyperlipidemic potential of ethanolic Avicennia marina leaves extract supported by metabolic profiling. Environ Sci Pollut Res 28(21):27207–27217
32. Sonboli A, Mojarrad M, Ebrahimi SN, Enayat S (2010) Free radical scavenging activity and total phenolic content of methanolic extracts from male inflorescence of Salix aegyptiaca grown in Iran. Iran J Pharm Res IJPR 9(3):293
33. Al-Warhi T, Elmaidomy AH, Maher SA, Abu-Baih DH, Selim S, Albqmi M et al (2022) The wound-healing potential of Olea europaea L. cv. Arbequina leaves extract: an integrated in vitro, in silico, and in vivo investigation. Metabolites 12(9):791
34. Ozbilgin S, Ozkardesler S, Akan M, Boztas N, Ozbilgin M, Ergur BU et al (2016) Renal ischemia/reperfusion injury in diabetic rats: the role of local ischemic preconditioning. BioMed Res Int 2016:1–9. https://doi.org/10.1155/2016/8580475
35. Al-Warhi T, Zahran EM, Selim S, Al-Sanea MM, Ghoneim MM, Maher SA et al (2022) Antioxidant and wound healing potential of Vitis vinifera seeds supported by phytochemical characterization and docking studies. Antioxidants 11(5):881
36. Sandhu SK, Kumar S, Raut J, Singh M, Kaur S, Sharma G et al (2021) Systematic development and characterization of novel, high drug-loaded, photostable, curcumin solid lipid nanoparticle hydrogel for wound healing. Antioxidants 10(5):725
37. Shady NH, Altemani AH, Altemani FH, Maher SA, Elrehany MA, Saber EA et al (2022) The potential of corchorus olitorius seeds buccal films for treatment of recurrent minor aphthous ulcerations in human volunteers. Molecules 27(20):7020
38. Hummon AB, Lim SR, Difilippantonio MJ, Ried T (2007) Isolation and solubilization of proteins after TRIzol® extraction of RNA and DNA from patient material following prolonged storage. Biotechniques 42(4):467–472
39. Boesenberg-Smith KA, Pessarakli MM, Wolk DM (2012) Assessment of DNA yield and purity: an overlooked detail of PCR troubleshooting. Clin Microbiol Newsl 34(1):1–6
40. Longo MC, Berninger MS, Hartley JL (1990) Use of uracil DNA glycosylase to control carry-over contamination in polymerase chain reactions. Gene 93(1):125–128
41. Livak KJ, Schmittgen TD (2001) Analysis of relative gene expression data using real-time quantitative PCR and the 2– ΔΔCT method. Methods 25(4):402–408
42. Ru J, Li P, Wang J, Zhou W, Li B, Huang C et al (2014) TCMSP: a database of systems pharmacology for drug discovery from herbal medicines. J Cheminform 6:13. https://doi.org/10.1186/1758-2946-6-13
43. Liu Z, Guo F, Wang Y, Li C, Zhang X, Li H et al (2016) BATMAN-TCM: a bioinformatics analysis tool for molecular mechanism of traditional Chinese medicine. Sci Rep 6:21146. https://doi.org/10.1038/srep21146
44. Davis AP, Wiegers TC, Wiegers J, Wyatt B, Johnson RJ, Sciaky D et al (2023) CTD Tetramers: a new online tool that computationally links curated chemicals, genes, phenotypes, and diseases to inform molecular mechanisms for environmental health. Toxicol Sci. https://doi.org/10.1093/toxsci/kfad069
45. UniProt C (2021) UniProt: the universal protein knowledgebase in 2021. Nucleic Acids Res 49(D1):D480–D489. https://doi.org/10.1093/nar/gkaa1100
46. Fishilevich S, Nudel R, Rappaport N, Hadar R, Plaschkes I, Iny Stein T et al (2017) GeneHancer: genome-wide integration of enhancers and target genes in GeneCards. Database (Oxford). https://doi.org/10.1093/database/bax028
47. Heberle H, Meirelles GV, da Silva FR, Telles GP, Minghim R (2015) InteractiVenn: a web-based tool for the analysis of sets through Venn diagrams. BMC Bioinf 16(1):169. https://doi.org/10.1186/s12859-015-0611-3
48. Szklarczyk D, Kirsch R, Koutrouli M, Nastou K, Mehryary F, Hachilif R et al (2023) The STRING database in 2023: protein-protein association networks and functional enrichment analyses for any sequenced genome of interest. Nucleic Acids Res 51(D1):D638–D646. https://doi.org/10.1093/nar/gkac1000
49. Shannon P, Markiel A, Ozier O, Baliga NS, Wang JT, Ramage D et al (2003) Cytoscape: a software environment for integrated models of

biomolecular interaction networks. Genome Res 13(11):2498–2504. https://doi.org/10.1101/gr.1239303
50. Berman HM, Westbrook J, Feng Z, Gilliland G, Bhat TN, Weissig H et al (2000) The protein data bank. Nucleic Acids Res 28(1):235–242. https://doi.org/10.1093/nar/28.1.235
51. Morris GM, Huey R, Lindstrom W, Sanner MF, Belew RK, Goodsell DS et al (2009) AutoDock4 and AutoDockTools4: automated docking with selective receptor flexibility. J Comput Chem 30(16):2785–2791. https://doi.org/10.1002/jcc.21256
52. Trott O, Olson AJ (2010) AutoDock Vina: improving the speed and accuracy of docking with a new scoring function, efficient optimization, and multithreading. J Comput Chem 31(2):455–461. https://doi.org/10.1002/jcc.21334
53. Jaghoori MM, Bleijlevens B, Olabarriaga SD (2016) 1001 Ways to run AutoDock Vina for virtual screening. J Comput Aided Mol Des 30(3):237–249. https://doi.org/10.1007/s10822-016-9900-9
54. Bao NC, Ty PV (2017) Long-chain compounds isolated from Lac Tien (Passiflora foetida L.). Hue Univ J Sci Nat Sci 126(1C):101–106
55. Engelbrecht J, Tursch B, Djerassi C (1972) A new sterol from an alcyonarian. Steroids 20(1):121–126
56. Rahelivao MP, Lübken T, Gruner M, Kataeva O, Ralambondrahety R, Andriamanantoanina H et al (2017) Isolation and structure elucidation of natural products of three soft corals and a sponge from the coast of Madagascar. Org Biomol Chem 15(12):2593–2608
57. Kim D-O, Chun OK, Kim YJ, Moon H-Y, Lee CY (2003) Quantification of polyphenolics and their antioxidant capacity in fresh plums. J Agric Food Chem 51(22):6509–6515
58. Landén NX, Li D, Ståhle M (2016) Transition from inflammation to proliferation: a critical step during wound healing. Cell Mol Life Sci 73(20):3861–3885
59. Krzyszczyk P, Schloss R, Palmer A, Berthiaume F (2018) The role of macrophages in acute and chronic wound healing and interventions to promote pro-wound healing phenotypes. Front Physiol 9:419
60. Cheng S-Y, Lin E-H, Huang J-S, Wen Z-H, Duh C-Y (2010) Ylangene-type and nardosinane-type sesquiterpenoids from the soft corals Lemnalia flava and Paralemnalia thyrsoides. Chem Pharm Bull 58(3):381–385
61. Alassass AA, Abubakr MS, Alarif WM, Ayyad S-EN, Mohammed A-EE (2022) Anti-inflammatory, antioxidant, cytotoxic activities, and sesquiterpenoid contents of Paralemnalia thyrsoides. Pharmacogn Mag 18(77):188–192
62. Lee Y-S, Duh T-H, Siao S-S, Chang R-C, Wang S-K, Duh C-Y (2017) New cytotoxic terpenoids from soft corals Nephthea chabroli and Paralemnalia thyrsoides. Mar Drugs 15(12):392
63. Huang C-Y, Su J-H, Chen B-W, Wen Z-H, Hsu C-H, Dai C-F et al (2011) Nardosinane-type sesquiterpenoids from the Formosan soft coral Paralemnalia thyrsoides. Mar Drugs 9(9):1543–1553
64. Alassass AAA, Abubakr MS, Ayyad S-EN, Mohammed E (2021) Chemical investigation and isolation of some constituents from Paralemnalia thyrsoides. World J Pharm Sci 9:1–5
65. Paola G, Frances N, David T, Elisabeth K (2008) The role of oxygen in wound healing. Dermatol Surg 34:1159–1169
66. Boakye YD, Agyare C, Ayande GP, Titiloye N, Asiamah EA, Danquah KO (2018) Assessment of wound-healing properties of medicinal plants: the case of Phyllanthus muellerianus. Front Pharmacol 9:945
67. Khan H, Khan AL, Hussain J, Adnan M, Hussain I, Khan T et al (2008) Review sesquiterpenes: the potent antioxidants. Biol Sci PJSIR 51(6):343–350
68. Siwik DA, Pagano PJ, Colucci WS (2001) Oxidative stress regulates collagen synthesis and matrix metalloproteinase activity in cardiac fibroblasts. Am J Physiol Cell Physiol 280(1):C53–C60
69. Rodriguez-Menocal L, Shareef S, Salgado M, Shabbir A, Van Badiavas E (2015) Role of whole bone marrow, whole bone marrow cultured cells, and mesenchymal stem cells in chronic wound healing. Stem Cell Res Ther 6(1):1–11
70. Singh K, Agrawal NK, Gupta SK, Sinha P, Singh K (2016) Increased expression of TLR9 associated with pro-inflammatory S100A8 and IL-8 in diabetic wounds could lead to unresolved inflammation in type 2 diabetes mellitus (T2DM) cases with impaired wound healing. J Diabetes Complicat 30(1):99–108
71. Tang T, Yin L, Yang J, Shan G (2007) Emodin, an anthraquinone derivative from Rheum officinale Baill, enhances cutaneous wound healing in rats. Eur J Pharmacol 567(3):177–185
72. Pachuau L (2015) Recent developments in novel drug delivery systems for wound healing. Expert Opin Drug Deliv 12(12):1895–1909
73. Suguna L, Singh S, Sivakumar P, Sampath P, Chandrakasan G (2002) Influence of Terminalia chebula on dermal wound healing in rats. Phytother Res 16(3):227–231
74. Schultz GS, Ladwig G, Wysocki A (2005) Extracellular matrix: review of its roles in acute and chronic wounds. World wide wounds 2005:1–18
75. Sasaki M, Kashima M, Ito T, Watanabe A, Izumiyama N, Sano M et al (2000) Differential regulation of metalloproteinase production, proliferation and chemotaxis of human lung fibroblasts by PDGF, interleukin-1β and TNF-α. Mediators Inflamm 9(3–4):155–160
76. Sano C, Shimizu T, Tomioka H (2003) Effects of secretory leukocyte protease inhibitor on the tumor necrosis factor-alpha production and NF-κB activation of lipopolysaccharide-stimulated macrophages. Cytokine 21(1):38–42
77. Pakyari M, Farrokhi A, Maharlooei MK, Ghahary A (2013) Critical role of transforming growth factor beta in different phases of wound healing. Adv Wound Care 2(5):215–224
78. Wan R, Weissman JP, Grundman K, Lang L, Grybowski DJ, Galiano RD (2021) Diabetic wound healing: The impact of diabetes on myofibroblast activity and its potential therapeutic treatments. Wound Repair Regen 29(4):573–581
79. El Baassiri M, Dosh L, Haidar H, Gerges A, Baassiri S, Leone A et al (2022) Nerve growth factor and burn wound healing: update of molecular interactions with skin cells. Burns 49(5):989–1002
80. Komi DEA, Khomtchouk K, Santa Maria PL (2020) A review of the contribution of mast cells in wound healing: involved molecular and cellular mechanisms. Clin Rev Allergy Immunol 58:298–312
81. Palomares O, Martin-Fontecha M, Lauener R, Traidl-Hoffmann C, Cavkaytar O, Akdis M et al (2014) Regulatory T cells and immune regulation of allergic diseases: roles of IL-10 and TGF-β. Genes Immun 15(8):511–520

Publisher's Note